Supporting Information

Experimental Methods

Materials. All chemicals were purchased from Sigma-Aldrich and used as received. Deionized water was used throughout.

Peptide Coupling. The compound with a free carboxylic acid group (the acid) was dissolved in $CHCl_3$ (20 mL/1 g of solid) with the addition of N-methyl morpholine (NMM) until a transparent solution was obtained. Isobutyl chloroformate (IBCF, 1.2 equivalents) was added and the solution stirred on ice for 10 minutes. The compound with a free amine group (the amine, 1 molar equivalent) was dissolved separately in $CHCl_3$ (20 mL/1 g of solid) with the addition of NMM (aliquots of 5 equivalents until a transparent solution was obtained). Following activation of the acid, the amine solution was added, and the reaction mixture stirred on ice overnight. The following day, the reaction mixture was washed sequentially with HCl (1 M, 1.25 x the volume of the reaction mixture), water (1.25 x the volume of the reaction mixture) and brine (1.25 x the volume of the reaction mixture). The organic phase was dried with $MgSO_4$, filtered and the solvent removed in vacuo to give the product. Where required, the product was purified by column chromatography in a 2:8, 1:9 or 1:99 EtOAc:DCM solvent system, depending on separation from impurities on a TLC plate.

Boc Deprotection. The Boc-protected peptide was dissolved in $CHCl_3$ (10 mL/1 g of solid) and trifluoroacetic acid (TFA) added such that the ratio of TFA:$CHCl_3$ was 1:2. The reaction was stirred overnight at room temperature before being poured into a large excess of Et_2O and stirred vigorously overnight. The resulting precipitate was filtered under vacuum to give the product as a solid. The product was dried further by azeotropic distillation with CH_3CN. Where required, the product was washed by trituration in Et_2O.

Methyl Ester Deprotection. The methyl ester-protected peptide was dissolved in tetrahydrofuran (THF, 10 mL/1 g of solid). LiOH (5 molar equivalents) was dissolved separately in water so that the ratio of THF:water was 1:1. The LiOH solution was added to the peptide solution and the reaction stirred at room temperature. The reaction was monitored by TLC using a suitable solvent system (generally 1:9 EtOAc:DCM). After the reaction had gone to completion, the reaction mixture was poured into a large excess of 1 M HCl and stirred vigorously overnight. The resulting precipitate was filtered under vacuum, washed with plentiful deionised water and dried by azeotropic distillation with CH_3CN to give the product as a solid. Where required, the product was washed by trituration in Et_2O.

Preparation of micellar suspensions. Stock suspensions (10 mg/mL) of each component was prepared in water with the addition of 1 molar equivalent of NaOH (0.1 M). The stock suspensions were stirred overnight to ensure complete dispersion of the molecules. The pH of each stock suspension was adjusted to 10.5 before preparing the multicomponent suspensions. The multicomponent suspensions were prepared by mixing calculated volumes of the stock suspensions of the two components in each multicomponent system, such that a total gelator concentration of 10 mg/mL was maintained while achieving concentration ratios of 7.5 mg/mL:2.5 mg/mL, 5 mg/mL:5 mg/mL and 2.5 mg/mL:7.5 mg/mL. Multicomponent suspensions were stirred for 2 hours to ensure thorough mixing of components. The pH of all suspensions was adjusted to 10.5 again before analysis or gel formation. Where possible, the same stock solution of each component was used for all data that would be directly compared e.g. the same stock solutions were used for all viscosity measurements.

pH measurements. The pH of samples was measured using a FC200 pH probe from Hanna instruments. The pH meter was calibrated using pH 4.01, 7.01 and 10.01 buffer solutions. The probe was rinsed with deionised water between measurements.

Preparation of gels by reduction in pH using GdL. Single and multicomponent micellar suspensions were prepared as previously described. Gel samples were prepared in 7 mL Sterilin vials by addition of 2 mL of the required single or multicomponent micellar suspension (10 mg/mL, pH 10.5) to 32 mg of solid GdL (16 mg/mL of GdL). In cases where the gelator concentration was 5 mg/mL, the GdL concentration was reduced to 8 mg/mL. The vials were swirled briefly by hand to ensure complete dissolution of GdL then left to stand overnight undisturbed.

Viscosity measurements. Viscosity measurements were performed using an Anton Paar Physica 101 or 301 rheometer using a CP50 cone (cone angle: 0.995 °) and plate (sample volume ~1 mL). ~1 mL of solution was transferred onto the plate by pouring. Viscosity values were collected at shear rates ranging from 1-100 or 1-1000 s^{-1}. Measurements were performed in each condition in duplicate or triplicate and the average calculated. All viscosity measurements were performed at a temperature of 25 °C.

Strain and Frequency Sweeps. All rheological measurements were carried out using an Anton Paar Physica MCR 301 rheometer at a defined temperature/series of temperatures. Strain, frequency and time sweeps were performed using cup and vane geometry (ST10-4V-8.8/97.5-SN18190) with a gap height of 1.8 mm. Strain sweeps were performed at a frequency of 10 rad/s from 0.01% to 1000% strain. Frequency sweeps were performed at 0.1% strain from 1 rad/s to 100 rad/s frequency. Time sweeps were performed at 0.1% strain and 10 rad/s frequency. All samples were prepared as previously described in a 2 mL volume in 7 mL Sterilin vials.

Circular Dichroism. Circular dichroism (CD) was measured using a Chirascan VX CD spectrometer (Applied Photophysics Limited, U.K.) using a quartz cell with a 0.01 mm path length and the following parameters: scanning mode, continuous; scanning speed, 120 nm/min and bandwidth, 1 nm. All CD

data are presented as ellipticity and recorded in millidegree (mdeg). Absorbance and HV spectra were recorded concomitantly with CD spectra. Spectra were obtained at a 2 min interval from 180 to 300 nm or 180 nm to 500 nm at a speed of 120 nm/min. All spectra were recorded in triplicate and averaged with the exception of the temperature-variable CD experiments (Chapter 3). These were recorded as a single measurement on the same sample at each temperature. CD spectra were recorded at intervals of 5 ℃ at temperatures ranging from 25 ℃ to 95 ℃ (the upper limit of the CD spectrometer).

UV-Vis Spectroscopy. Solution UV-vis absorption data were obtained with an Agilent Cary 60 UV-vis spectrophotometer. The samples were prepared as described above and transferred into a 0.01 mm quartz cuvette.

NMR spectroscopy. NMR spectroscopy experiments were carried out on a Bruker DPX 400MHz spectrometer at 300 K. All compounds were dissolved in d_6-DMSO.

Small Angle Neutron Scattering. Solutions were prepared as described above in D_2O using NaOD to adjust the pH. Scattering length density (SLD) values were calculated using the NIST neutron activation and scattering calculator,[1] assuming a density o 1.55 g/cm^3. SLD values used for all systems are shown in Table S1. For multicomponent systems, the SLD values were calculated based on the ratio of the two components.

System	SLD (x 10^{-6} Å^{-2})
2NapFF 10 mg/mL	2.730
7MeO2NapFV 10 mg/mL	2.357
7MeO2NapFV 5 mg/mL: 2NapFF 5 mg/mL	2.543
1NapVV 10 mg/mL	2.081
1NapVV 5 mg/mL: 2NapFF 5 mg/mL	2.406
CarbFV 10 mg/mL	2.553
CarbFV 5 mg/mL: 2NapFF 5 mg/mL	2.642
CarbIF 10 mg/mL	2.463
CarbIF 5 mg/mL: 2NapFF 5 mg/mL	2.597
D_2O (solvent)	6.393

Table S1. SLD values used when fitting SANS data for all the systems studied.

SANS data was collected by R. E. Ginesi (UofG, UK), E. R. Draper (UofG, UK) and D. J. Adams (UofG, UK). Data were fit by S. Bianco (UofG, UK) and L. J. Marshall. Solutions were prepared as described above in D_2O and NaOD (0.1 M). SANS measurements were formed using the SANS2D and ZOOM instrument (ISIS, Rutherford Appleton Laboratory, Didcot, UK) under experiment numbers RB220189 for gels and RB2220215 for solutions, using a wavelength band of 0.9 to 13 Å to access a q range of 0.004 to 0.7 Å-1. Solutions and gels were measured in 2 mm path length UV spectrophotometer grade quartz cuvettes (Hellma). The samples were placed in a temperature-controlled sample rack

during the measurements. All data was collected at 25 °C. Gels formed using GdL were prepared in a Sterilin vial and quickly transferred to the cuvettes, before being placed on the rack.

The data was reduced to 1D scattering curves of intensity vs Q. using the facility provided software. The electronic background was subtracted, the full detector images for all data were normalised and scattering from the empty cell was subtracted. The scattering from D2O was also measured and subtracted from the data using the Mantid software package installed inside the ISIS virtual machines, IDAaaS.[2] The instrument-independent data were then fitted to the models discussed in the text using the SasView software package (version 5.0.3).[3]

PXRD. X-ray diffraction patterns were collected on a Malvern Panalytical Empyrean with a PIXcel3D-Medipix3 1x1 detector using Cu Kα radiation (wavelength = 1.541874 Å).

Discussion of SANS data at high pH

Inclusion of a power law component improved the quality of the fit for several of the systems. We expect the inclusion of a power law allows us to take into account interactions between structures at longer length scales. A power law was only included when necessary to fully capture the data to avoid overfitting. A superior fit was achieved for many of the systems studied when the length was set to an arbitrary value outside the range available by SANS. Here we use 5000 Å. Inclusion of polydispersity in the radius parameter allowed us to fully capture the data at Q ≈ 0.1 $Å^{-1}$ for several data sets. In all cases, the background value for the fit was entered manually.

The axis ratio obtained for the 7MeO2NapFV 10 mg/mL single component system was almost exactly 2 (Table S2, ESI). This suggests that the SANS data corresponds to two cylinders laterally associated with one another which could explain the difficulty faced fitting this data. It is also possible that 7MeO2NapFV 10 mg/mL forms helical tapes as previous work has shown that the best fit for these structures arises from an elliptical cylinder model.[4] Since the SANS data from the 1NapVV 10 mg/mL single component system was fit to a power law only we expect that the structures formed by 1NapVV are too large to be measured by SANS or that the structures are not sufficiently persistent to provide a strong scattering signal.[5]

The parameters obtained for 7MeO2NapFV 5 mg/mL:2Nap-(*SS*)-FF 5 mg/mL at high pH are within fitting error of those obtained for 2Nap-(*SS*)-FF 10 mg/mL (Table S2, ESI). This suggests complete co-assembly of the two components with 2Nap-(*SS*)-FF directing assembly.[6] A power law component was included to completely capture the SANS data collected from the 7MeO2NapFV 5 mg/mL:2Nap-(*SS*)-FF 5 mg/mL sample. Inclusion of a power law suggests there are more interactions occurring at longer length scales in the multicomponent system. The length of the 7MeO2NapFV 5 mg/mL:2Nap-(*SS*)-FF 5 mg/mL sample could be fit to a value within the range of SANS. This could be the fitting software

picking up on the Kuhn length of the sample as we would expect that the structures formed by these systems would have lengths out with the range accessible by SANS.[7] The inclusion of polydispersity of the radius was no longer required in the 7MeO2NapFV 5 mg/mL:2Nap-(*SS*)-FF 5 mg/mL sample, suggesting increased homogeneity of the structures in the multicomponent sample.

SANS data collected from 2Nap-(*RS*)-FF systems were challenging to fit and often gave high Chi2 values, despite the fits being reasonable by eye. Fitting the 7MeO2NapFV 5 mg/mL:2Nap-(*RS*)-FF 5 mg/mL SANS data to a hollow cylinder model combined with a power law provided the best fit (Table S3, ESI). Attempts to fit all parameters at once gave high error for the A scale and an unrealistically small value for the thickness, which would suggest the structures are not actually hollow. However, none of the other models or combinations of models gave good quality fits according to residuals, error values and the proximity of the fit to the data by eye. Inputting the parameters from 2Nap-(*RS*)-FF 10 mg/mL gave a reasonable fit apart from at low Q. Inclusion of a power law component to hollow cylinder parameters from 2Nap-(*RS*)-FF RS 10 mg/mL further improved the fit. Manually increasing the power law value improved the fit at low Q but slightly reduced the quality of fit at high Q. From the final fit, we expect co-assembly is taking place with 2Nap-(*RS*)-FF directing assembly. Attempts to fit this data to a combination of cylinder models did not improve the quality of the fit, confirming that 7MeO2NapFV and 2Nap-(*RS*)-FF are not self-sorting.

As with 7MeO2NapFV, the SANS data collected from the 1NapVV multicomponent systems were fit to the same hollow cylinder model as the 2Nap-(*SS*)-FF 10 mg/mL (Table S2, ESI) and 2Nap-(*RS*)-FF 10 mg/mL (Table S3, ESI) single component systems with the inclusion of a power law to allow capture of the data at low Q. The parameters obtained from fits of the multicomponent systems are very similar to those obtained for the 2NapFF single component systems of the corresponding chirality, suggesting co-assembly with 2NapFF directing assembly. Slight differences are observed in the 1NapVV multicomponent systems compared to the 2NapFF single component systems. Fits of the structures in the 1NapVV 5 mg/mL:2Nap-(*RS*)-FF 5 mg/mL multicomponent system gave almost half the thickness of those in the 2Nap-(*RS*)-FF 10 mg/mL single component system. Polydispersity was included to improve the quality of the fit obtained for the multicomponent system (Table S3, ESI). This suggests the presence of cylinders with a range of values for the radius. A power law component was included in the fit for the multicomponent systems of both 2NapFF diastereomer. The values for the power law were set manually as this provided a fit of better quality at low Q (by eye) than the value obtained from automatic fitting.

When the CarbFV 5 mg/mL:2Nap-(*SS*)-FF 5 mg/mL multicomponent system is fitted to a hollow cylinder model, the radius obtained is the average of the values obtained when the system is fit to a combined model of two hollow cylinders (Table S4, ESI). When fitting to a combined model (hollow cylinder + hollow cylinder), we used the parameters obtained from each component alone as a starting

point. The parameters obtained from the combined hollow cylinder model fit do not match those obtained from SANS data collected from each component at 10 mg/mL since concentration (the multicomponent systems only have 5 mg/mL of each component) and the presence of a second component will affect the structures formed. It should be noted that self-sorting may also be occurring to some degree.

Despite providing a fit of similar quality by eye to the hollow cylinder + power law model (Fig 6aiii), the hollow cylinder-hollow cylinder combined model fit had a higher Chi2 value and had larger parameter error values (Table S4, ESI). The CD spectra of the CarbFV multicomponent systems did not show the expected behaviour for a self-sorted system and instead indicates that CarbFV and 2Nap-(*SS*)-FF undergo co-assembly directed by CarbFV. This is further corroborated by the similarities between the parameters obtained from fitting SANS data from CarbFV 10 mg/mL and SANS data from CarbFV 5 mg/mL:2Nap-(*SS*)-FF 5 mg/mL.

Fitting the SANS data from the CarbIF 5 mg/mL:2Nap-(*SS*)-FF 5 mg/mL multicomponent system to a hollow cylinder model provided the best quality fit compared to all other cylinder models. The parameters obtained did not resemble those from either system alone. This could be mean co-assembly is taking place, resulting in the formation of new structures, or that the two components are self-sorting, and the reduced concentration is having a significant effect on the structures formed by each component.

To probe this further, we tried fitting the data to a variety of combined models with at least one hollow cylinder to account for 2Nap-(*SS*)-FF since we know from previous experiments[8-11] that 2Nap-(*SS*)-FF forms hollow cylinders at a concentration of 5 mg/mL. The data could be fit to a range of model combinations: hollow cylinder-cylinder, hollow cylinder + hollow cylinder, hollow cylinder + elliptical cylinder, hollow cylinder + flexible cylinder, hollow cylinder + flexible elliptical cylinder. All these combinations provided fits of similar quality by eye, with Chi2 values similar to or less than that obtained from fitting to a single hollow cylinder model. A combination of a hollow cylinder model and a flexible cylinder model gave the lowest parameter error values and one of the lowest Chi2 values (Table S4, ESI).

Discussion of SANS data at low pH

As with the SANS data collected from samples at high pH, we attempted to fit all data sets to all available standard cylinder models in order to identify the most suitable model for each set of data. Fitting SANS data collected from the 2Nap-(*SS*)-FF 10 mg/mL gel sample did not yield the expected parameters based on previous work.[9, 10] Manually entering the expected values greatly decreased the quality of the fit. We do not know the reason behind this. Inclusion of polydispersity in the radius

parameter allowed us to fully capture the data at Q = 0.1 $Å^{-1}$. This was necessary for most of the systems in the gel state.

In most cases, the value obtained for length during fitting was beyond the scale available by neutron scattering. As before, we set the length for these data sets to 5000 Å. Changing from this value does not significantly affect the quality of the fit. Inclusion of a power law helps us to capture scattering contribution from the gel network.[10] The power law is dominant at low Q. The values for axis ratio in elliptical models might originate from lateral association of fibres in the gel network.[11]

Fitting the SANS data from the 2Nap-(*SS*)-FF 10 mg/mL single component system to a flexible elliptical cylinder model combined with a power law provided the best fit (Fig. 8). The 7MeO2NapFV 10 mg/mL single component system was also best fit to a flexible elliptical cylinder model but without the power law component (Fig. 8ai). , fits obtained using the parameters from the 2Nap-(*SS*)-FF single component system did not match the data. Fitting all the parameters together after inputting the values from the 2Nap-(*SS*)-FF single component fit gave an axis ratio of 1 suggesting the structures formed in the multicomponent system are not elliptical and are therefore fundamentally different to those formed by the single component systems. The 7MeO2NapFV 5 mg/mL: 2Nap-(*SS*)-FF 5 mg/mL multicomponent system was instead fitted to a flexible cylinder model (Fig. 8ai). Co-assembly of the two components is therefore causing a significant difference in assembly on a reduction in pH and therefore the primary structures of the gel network.

The 1NapVV 10 mg/mL gel has high polydispersity (Table S6, ESI). This implies that not all primary structures present in the gel have the same radius. The SANS data from the 1NapVV 5 mg/mL:2Nap-(*SS*)-FF multicomponent system was fitted by first inputting the parameters from 2Nap-(*SS*)-FF single component system then fitting all the parameters together. This method of fitting provided the best fit according to Chi^2 value, parameter errors, residuals and how the fit looked by eye. This suggests that the 2Nap-(*SS*)-FF directed co-assembly observed at high pH persists in the gel state at low pH. Despite having similar behaviour at high pH, the 1NapVV and 7MeO2NapFV multicomponent systems exhibit different behaviour on a reduction in pH.

The reduced Chi^2 values obtained from fitting SANS data from 2Nap-(*RS*)-FF single and multicomponent systems are high in both the sol and gel states. However, the fits obtained look reasonable by eye and the parameters obtained from the fits have small error values. It is interesting that 2Nap-(*RS*)-FF maintains a hollow cylinder structure going from the sol state at high pH to the gel state at low pH as this is not observed with 2Nap-(*SS*)-FF. The only parameter that changes considerably going from the sol state to the gel state is the thickness of the hollow cylinder, which almost doubles (Table S7, ESI). This could indicate lateral association of the fibres during formation of the gel network.[11] Experiments following small-angle scattering with time during gelation could be helpful in the future.

Co-assembly of 2Nap-(*RS*)-FF 5 mg/mL with 7MeO2NapFV 5 mg/mL causes significant changes to the parameters of the fit as compared to the 2Nap-(*RS*)-FF 10 mg/mL single component system (Table S7, ESI). The model used to fit the SANS data from the multicomponent system is the same as the model used for the 2Nap-(*RS*)-FF 10 mg/mL single component system, suggesting 2Nap-(*RS*)-FF is directing assembly at low pH. However, the parameters obtained from the fit are notably different to those obtained from the 2Nap-(*RS*)-FF 10 mg/mL single component system, showing that co-assembly with 7MeO2NapFV changes the structures formed.

The SANS data from the 1NapVV 5 mg/mL:2Nap-(*RS*)-FF 5 mg/mL multicomponent system was fitted to a flexible elliptical cylinder, the same model as was used for the 1NapVV single component system, suggesting that 1NapVV rather than 2Nap-(*RS*)-FF is directing assembly at low pH (Table S7, ESI). Co-assembly of 1NapVV with 2Nap-(*RS*)-FF resulted in formation of structures with significantly smaller radii than those formed by 1NapVV alone. We were also able to fit the length of these structures, rather than setting it to 5000 Å. It appears that, although 2Nap-(*RS*)-FF seems to direct assembly at high pH, 1NapVV takes over at low pH.

We tried to combine cylinder models for the CarbFV 5 mg/mL:2Nap-(*SS*)-FF 5 mg/mL system to investigate whether the self-sorting is taking place at low pH. While the fits looked good by eye and had low Chi^2 values (~2) for flexible elliptical cylinder + cylinder model, flexible cylinder and flexible elliptical cylinder models, the values obtained for the axis ratios were unreasonably high (between 7 and 11), depending on the models chosen. The data was best fitted to an elliptical cylinder combined with a power law (Fig. 8aiii); this is different to either component alone. This information suggests that co-assembly is taking place between these components at low pH.

The CarbFV 5 mg/mL:2Nap-(*RS*)-FF 5 mg/mL multicomponent system showed the same behaviour as its 2Nap-(*SS*)-FF counterpart: we achieved the best quality fit for the CarbFV 5 mg/mL:2Nap-(*RS*)-FF 5 mg/mL multicomponent system using an elliptical cylinder model combined with a power law (Fig. 8biii). We tried fitting the data to the same models as each component alone, starting with the parameters obtained for the corresponding component. Neither provided suitable fits for the multicomponent data. This shows that co-assembly is resulting in the formation of new structures that do not resemble either component. From SANS data collected at high pH, it appears that co-assembly is arising on gelation from an initially self-sorted system.

A flexible cylinder model combined with a power law gave the best fit for the SANS data from CarbIF 5 mg/mL:2Nap-(*SS*)-FF 5 mg/mL multicomponent system compared to all other single cylinder models. We note that the fit did not capture the line shape exactly at low Q (Fig 8.). Fitting the data to a hollow cylinder model combined with a flexible elliptical cylinder model allowed us to capture the line shape more accurately at high Q, but the fit had a higher Chi2 value. The radius and thickness values for the hollow cylinder component had to be entered manually to better emulate the line shape between 0.1 and

0.3 Q. This was the only combined cylinder model we were able to achieve the correct line shape with. It is difficult to rationalise how hollow cylinders may be forming from this system. It is also important to be cautious of over-fitting as combined models add extra parameters. We therefore conclude that the CarbIF 5 mg/mL:2Nap-(*SS*)-FF 5 mg/mL multicomponent system also transitions from self-sorting in the micellar phase at high pH to co-assembly at low pH in the gel state. Without selectively deuterated experiments and some form of imaging, we cannot conclude for certain what is happening in these systems.

The CarbIF 5 mg/mL:2Nap-(*RS*)-FF 5 mg/mL multicomponent system showed the same behaviour as the CarbFV multicomponent systems. The SANS data from this system were best fit to a flexible cylinder model combined with a power law (Fig. 8biv). While combining two cylinder models gave fits of similar quality according to Chi^2 value, error values and evaluating the fit by eye, the values obtained for the axis ratios were unusually high (between 7 and 11). We therefore conclude that, like the CarbFV 5mg/mL:2Nap-(*RS*)-FF 5 mg/mL multicomponent system, CarbIF 5mg/mL:2Nap-(*RS*)-FF also transitions from self-sorting at high pH to co-assembly with 2Nap-(*RS*)-FF when the pH is reduced.

Discussion of rheology data

The 7MeO2NapFV 10 mg/mL single component system forms gels with higher stiffness $(G')^{12}$ and tanδ $(G''/G')^{12}$ than 2Nap-(*SS*)-FF 10 mg/mL (Fig. 9ai). The 7MeO2NapFV 7.5 mg/mL:2Nap-(*SS*)-FF 2.5 mg/mL multicomponent gels have even greater stiffness and tanδ than the 7MeO2NapFV 10 mg/mL gels.

Incorporating a small proportion of 2Nap-(SS)-FF into the system increases the solid-like behaviour of the system. As 2Nap-(SS)-FF concentration increases, the stiffness and tanδ of the gels decreases. The 7MeO2NapFV 2.5 mg/mL:2Nap-(SS)-FF 7.5 mg/mL multicomponent gels have similar G′ and G″ values to the 2Nap-(SS)-FF 10 mg/mL single component gels, suggesting 2Nap-(SS)-FF dictates assembly at this concentration ratio. 1NapVV 10 mg/mL gels have lower stiffness and elasticity than 2Nap-(SS)-FF 10 mg/mL (Fig. 9aii). All the 1NapVV multicomponent systems have greater stiffness and elasticity than the single component systems, with 1NapVV 5 mg/mL:2Nap-(SS)-FF 5 mg/mL having the highest G′ and G″ values. This exemplifies how preparation of multicomponent systems and optimisation of concentration ratio can be used to enhance the mechanical properties of a chosen system. The 7MeO2NapFV and 1NapVV systems exhibit different behaviour in the gel state, despite their similarities in the sol state. 1NapVV being less similar to 2Nap-(SS)-FF than 7MeO2NapFV at the molecular level and the differences in the primary structures formed by these molecules in the gel state likely contribute to these differences to some extent.

CarbFV 10 mg/mL and CarbIF 10 mg/mL have lower G′ and G″ values than 2Nap-(SS)-FF 10 mg/mL (Fig. 9aiii and Fig. 9aiv). All the CarbFV multicomponent systems have lower G′ and elasticity than the single component systems. G′ increases with increasing 2Nap-(SS)-FF concentration. This example shows that preparation of multicomponent systems can also be used to reduce the stiffness of a system and, again, concentration ratio of components can be used to fine-tune the changes in mechanical properties. The CarbIF multicomponent systems showed a similar trend in stiffness and elasticity. This highlights the importance of the N-terminal capping groups chosen for each component during design of gelator-gelator multicomponent systems.

Strain sweeps provide valuable information about the mechanical properties of a gel in addition to moduli values. The strain value at which G′ begins to deviate from linear (the yield strain)35 tells us the strain at which the gel network begins to break down. The strain value at which G″ crosses over G′ (the flow point) tells us where the gel network has completely broken down and transitioned from a viscoelastic solid to a liquid.36 These values therefore tell us about the strength of the gel network.

Gels formed from 7MeO2NapFV alone have greater flow point than those formed from 2Nap-(SS)-FF alone, but a lower yield strain (Fig. 9bi). This suggests that while the network of 7MeO2NapFV gels begins to break down at a lower strain value, the network does not completely collapse until much greater strain is applied. Different behaviour in response to applied strain can be useful in different situations. Preparation of 7MeO2NapFV:2Nap-(SS)-FF multicomponent systems with concentration ratios 7.5:2.5 and 5:5 (mg/mL:mg/mL) reduces the mechanical strength of the gels formed compared to the single component systems. The 7MeO2NapFV 2.5 mg/mL:2Nap-(SS)-FF 7.5 mg/mL gels had the same yield strain and flow point values to the 2Nap-(SS)-FF gels, further confirming that 2Nap-(SS)-FF has completely taken over assembly at this concentration ratio. This highlights the importance of the concentration of each component.

1NapVV alone has a considerably higher flow point than all the other systems (Fig. 9bii). Incorporation of 2Nap-(SS)-FF into the system reduces the flow point considerably. As the 2Nap-(SS)-FF concentration increases in the 7MeO2NapFV and 1NapVV multicomponent systems, the values for all mechanical properties measured begin to resemble those from 2Nap-(SS)-FF alone. This could be related to the conclusions drawn from SANS, which shows that these systems co-assemble to form primary structures that resemble those formed by 2Nap-(SS)-FF alone at the same total gelator concentration.

The gels formed by CarbFV and CarbIF require high strain for the gel network to be completely broken down, signified by the larger flow point (Fig. 9biii and Fig. 9biv). The CarbFV 7.5 mg/mL:2Nap-(SS)-FF 2.5 mg/mL gels had lower yield strain and flow points than CarbFV alone (Fig. 9biii). As 2Nap-(SS)-FF concentration increases, both the yield strain and the cross-over point increase, resulting in the CarbFV 2.5 mg/mL:2Nap-(SS)-FF 7.5 mg/mL system having higher yield strain and a similar flow

point to 2Nap-(SS)-FF 10 mg/mL. While co-assembly at lower 2Nap-(SS)-FF concentrations disrupts the strength of the gel network, it is possible to achieve enhanced mechanical strength by optimising the concentration ratio of the two components while maintaining the total gelator concentration.

The CarbIF 7.5 mg/mL:2Nap-(*SS*)-FF 2.5 mg/mL multicomponent system has significantly greater yield strain and flow point than either component alone (Fig. 9biv). As 2Nap-(*SS*)-FF concentration increases, yield strain and cross-over point decrease. While the CarbIF 5 mg/mL:2Nap-(*SS*)-FF 5 mg/mL system has higher yield strain than 2Nap-(*SS*)-FF alone, it has lower flow point. The CarbIF 2.5 mg/mL:2Nap-(*SS*)-FF 7.5 mg/mL system has lower yield strain and flow point than either component alone. Again, the concentration ratio of the two components is clearly influencing the mechanical strength of the gels.

7MeO2NapFV 10 mg/mL also has higher stiffness and elasticity than 2Nap-(*RS*)-FF (Fig. 10ai). As the concentration of 2Nap-(*RS*)-FF in the system increases, G′ and elasticity decrease. Gels formed from the 2.5 mg/mL 7MeO2NapFV:7.5 mg/mL 2Nap-(*RS*)-FF 7.5 mg/mL multicomponent system have almost identical moduli values to 2Nap-(*RS*)-FF 10 mg/mL. This is the same as what was observed in the 7MeO2NapFV:2Nap-(*SS*)-FF multicomponent systems and agrees with observations from SANS data showing that 7MeO2NapFV co-assembles with 2Nap-(*RS*)-FF to form structures that resemble those formed by 2Nap-(*RS*)-FF alone.

1NapVV 10 mg/mL gels have much lower stiffness and elasticity than 2Nap-(*RS*)-FF 10 mg/mL (Fig. 10aii). The moduli values of the multicomponent gels are greater than those of the single component gels. The 1NapVV 5 mg/mL:2Nap-(*RS*)-FF 5 mg/mL has the highest moduli values, suggesting this is the optimum concentration ratio for maximising the mechanical properties of the gels. As with the 7MeO2NapFV multicomponent systems, changing the chirality of 2NapFF does not significantly change the trends observed in the mechanical properties of the gels.

The CarbFV:2Nap-(*RS*)-FF multicomponent gels show a clear trend of increasing moduli values with increasing 2Nap-(*RS*)-FF concentration (Fig. 10aiii). As the concentration of 2Nap-(*RS*)-FF increases and the concentration CarbFV decreases, the rheological properties of the gels change from resembling CarbFV to resembling 2Nap-(*RS*)-FF, which could suggest self-sorting. However, the moduli values exceed what would be expected from two separate additive networks (i.e. values in between the maximum concentrations of either component), suggesting co-assembly is taking place. This would agree with SANS experiments, where the data was best fit to a single model, showing that the two components are undergoing co-assembly.

The moduli values of the CarbIF:2Nap-(*RS*)-FF multicomponent systems are almost identical to CarbIF alone, until the CarbIF 2.5 mg/mL:2Nap-(*RS*)-FF 7.5 mg/mL system, which has very similar moduli values to 2Nap-(*RS*)-FF alone (Fig. 10aiv). SANS data suggests the CarbIF 5 mg/mL:2Nap-(*RS*)-FF 5 mg/mL system at least undergoes co-assembly. CarbIF therefore appears to direct co-assembly until the

2Nap-(*RS*)-FF concentration exceeds the CarbIF concentration. At which point 2Nap-(*RS*)-FF takes over.

The strength of the 2Nap-(*RS*)-FF multicomponent gels are strongly concentration dependent. The effect of concentration ratio varies depending on the identity of the second component despite all undergoing co-assembly, according to SANS data. The flow points of the 7MeO2NapFV:2Nap-(*RS*)-FF multicomponent gels increase with increasing 2Nap-(*RS*)-FF concentration (Fig. 10bi). While co-assembly reduces the strength of the gels at higher 7MeO2NapFV concentrations, the 2.5 mg/mL 7MeO2NapFV:2Nap-(*RS*)-FF 7.5 mg/mL system has similar yield strain and considerably higher flow point compared to the 2Nap-(*RS*)-FF 10 mg/mL gels.

The increased stiffness of the 1NapVV:2Nap-(*RS*)-FF multicomponent gels seems to compromise their strength, as seen by the considerably lower values obtained for the yield strain and flow point compared to the single component gels (Fig. 10bii). As with 7MeO2NapFV, yield strain increases with increasing 2Nap-(*RS*)-FF concentration. The 1NapVV 7.5 mg/mL:2Nap-(*RS*)-FF 2.5 mg/mL has an unexpectedly high flow point. There is no obvious reason for this.

CarbFV 10 mg/mL single component gels have significantly higher yield strain and flow point then 2Nap-(*RS*)-FF 10 mg/mL single component gels (Fig. 10biii). As 2Nap-(*RS*)-FF concentration in the multicomponent systems increases, the yield strain and flow point of the gels decrease. The 5 mg/mL:5 mg/mL and 2.5 mg/mL:7.5 mg/mL CarbFV:2Nap-(*RS*)-FF gels have lower strength than 2Nap-(*RS*)-FF alone. As with the 1NapVV multicomponent systems, this could be due to increased stiffness compromising gel strength.

The strength of the CarbIF multicomponent systems follow a similar trend to their stiffness. The multicomponent systems with CarbIF concentration greater than or equal to 2Nap-(*RS*)-FF concentration show enhanced strength that more closely resembles the strength of CarbIF alone at the same total gelator concentration (Fig. 10biv). The yield strain of CarbIF 2.5 mg/mL:2Nap-(*RS*)-FF 7.5 mg/mL multicomponent gels was very similar to that of the 2Nap-(*RS*)-FF 10 mg/mL single component gels. The flow point of these gels was unexpectedly high. In a mirror of the 1NapVV and CarbFV multicomponent systems, the increased strength of select CarbIF systems is paired with a reduction in stiffness.

The rheology data shows the vast array of possible outcomes from preparing multicomponent systems using a variety of gelators and by changing the chirality of one of the components. As already discussed, while we can achieve a wide variety of mechanical properties, it is practically impossible to predict the outcome of preparing multicomponent systems.

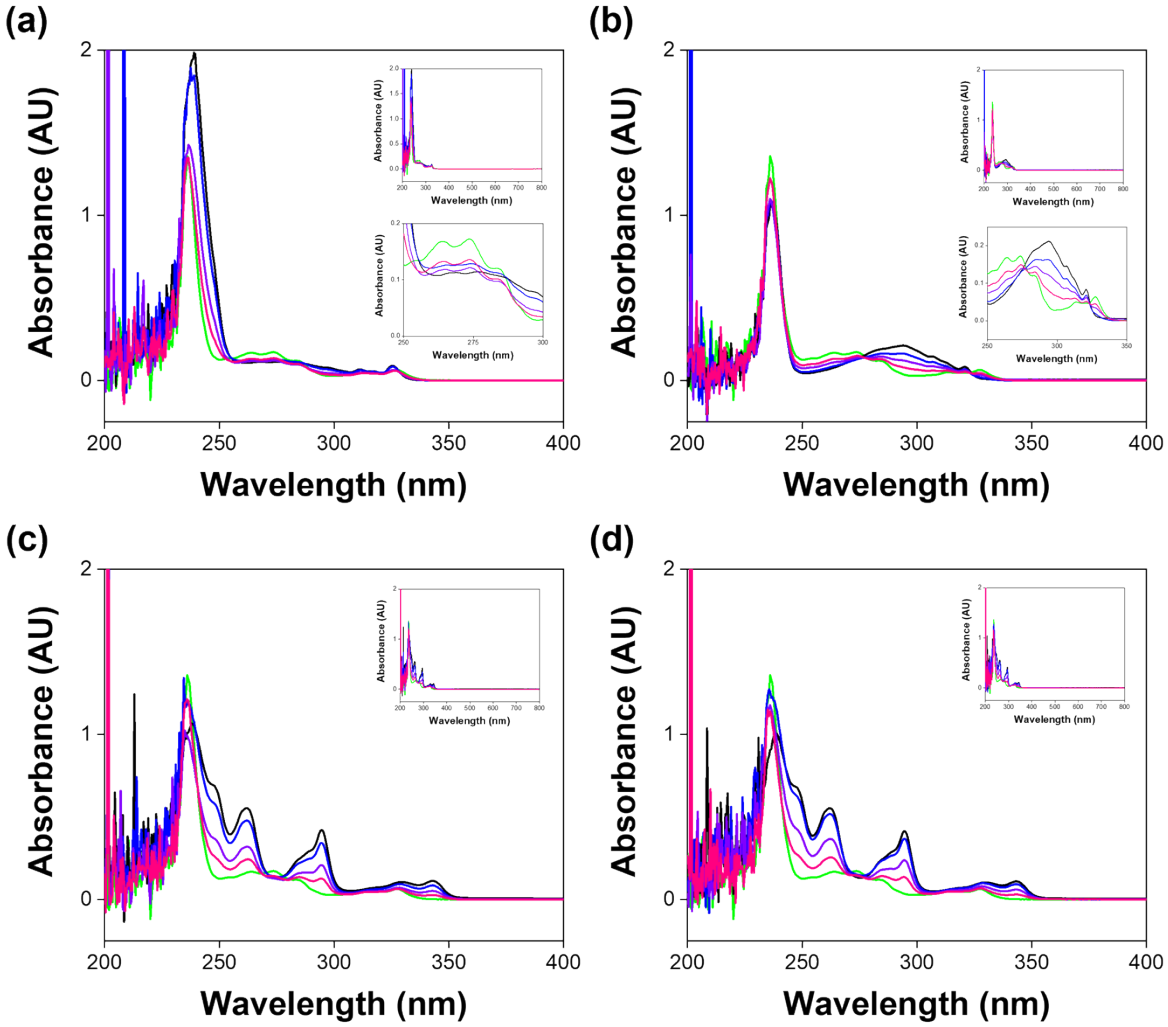

UV-Vis, Absorbance and HV data

Figure S1. UV-Vis absorption spectra recorded from single and multicomponent systems of (a) 7MeO2NapFV, (b) 1NapVV, (c) CarbFV and (d) CarbIF at concentration ratios second component:2Nap-(*SS*)-FF (mg/mL:mg/mL) of 10:0 (black), 7.5:2.5 (blue), 5:5 (purple) and 2.5:7.5 (pink) collected in DMSO. The data recorded from 2Nap-(*SS*)-FF 10 mg/mL (green) is shown in each spectrum for easy comparison with the multicomponent systems. The inserts show the entire spectrum (top) and selected regions to make them more visible (bottom).

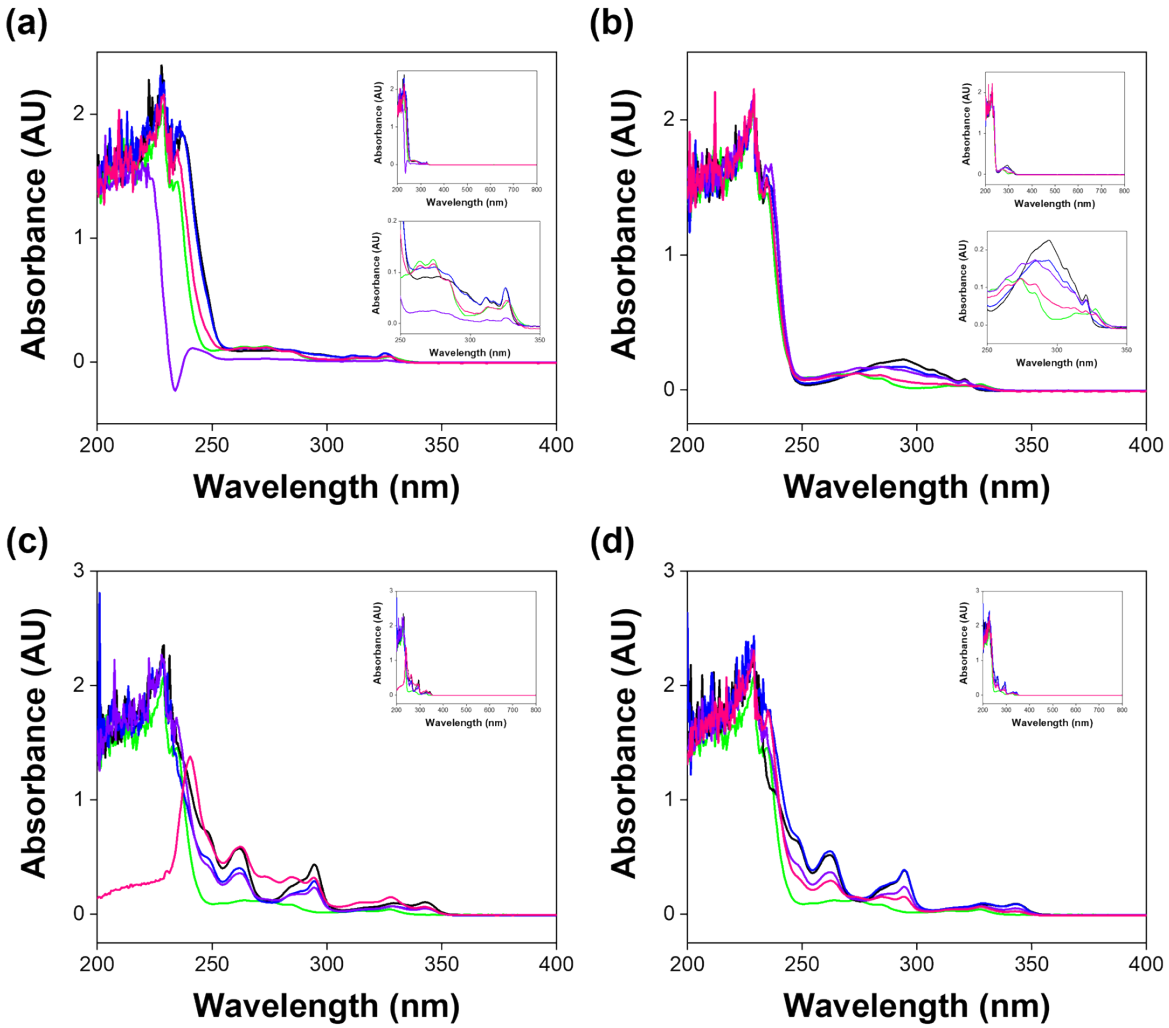

Figure S2. UV-Vis absorption spetra recorded from single and multicomponent systems of (a) 7MeO2NapFV, (b) 1NapVV, (c) CarbFV and (d) CarbIF at concentration ratios second component:2Nap-(*RS*)-FF (mg/mL:mg/mL) of 10:0 (black), 7.5:2.5 (blue), 5:5 (purple) and 2.5:7.5 (pink) collected in (i) DMSO. The data recorded from 2Nap-(*RS*)-FF 10 mg/mL (green) is shown in each spectrum for easy comparison with the multicomponent systems. The inserts show the entire spectrum (top) and selected regions to make them more visible (bottom).

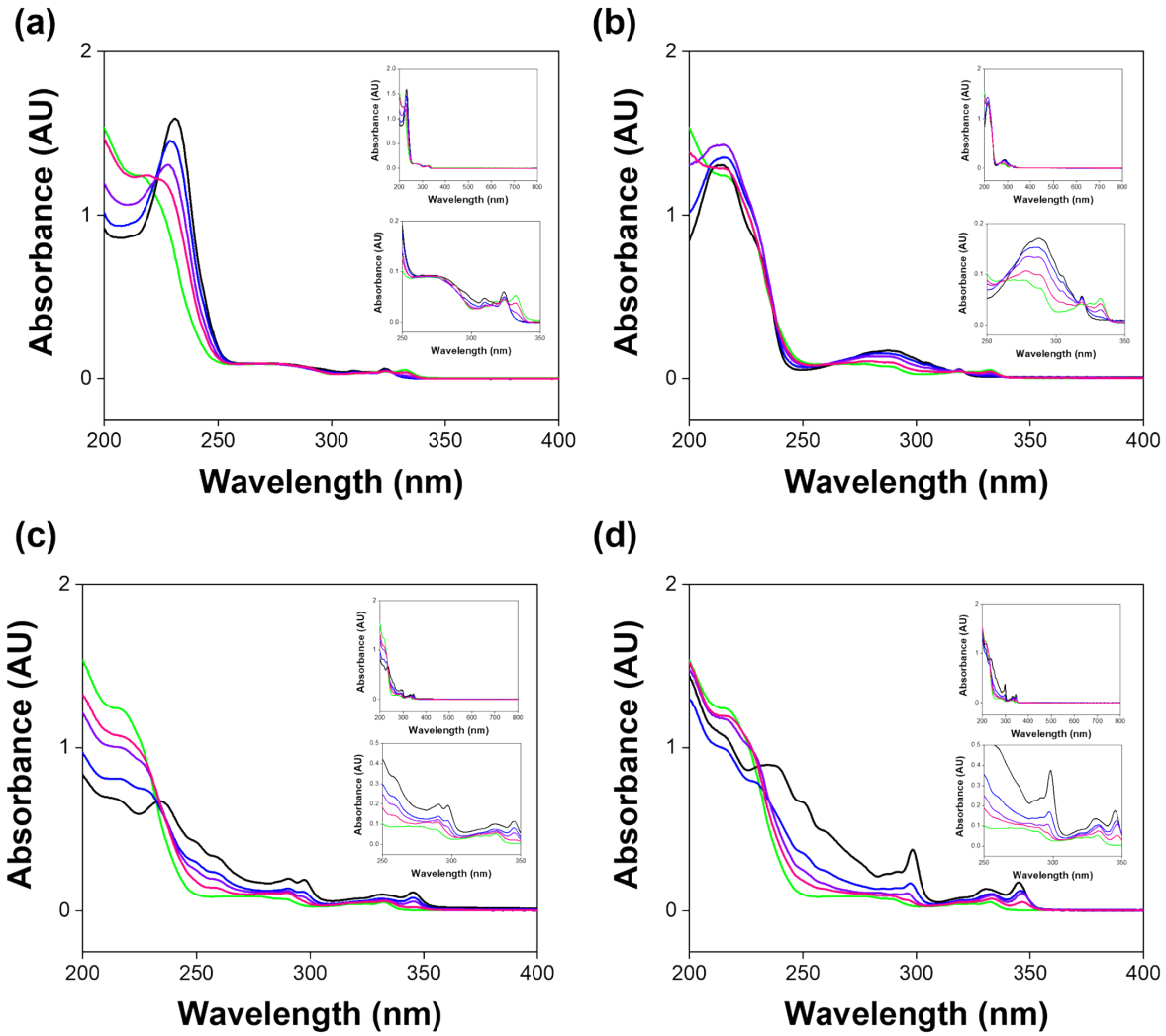

Figure S3. UV-Vis absorption spectra recorded from single and multicomponent systems of (a) 7MeO2NapFV, (b) 1NapVV, (c) CarbFV and (d) CarbIF at concentration ratios second component:2Nap-(*SS*)-FF (mg/mL:mg/mL) of 10:0 (black), 7.5:2.5 (blue), 5:5 (purple) and 2.5:7.5 (pink) collected in H_2O at pH 10.5. The data recorded from 2Nap-(*SS*)-FF 10 mg/mL (green) is shown in each spectrum for easy comparison with the multicomponent systems. The inserts show the entire spectrum (top) and selected regions to make them more visible (bottom).

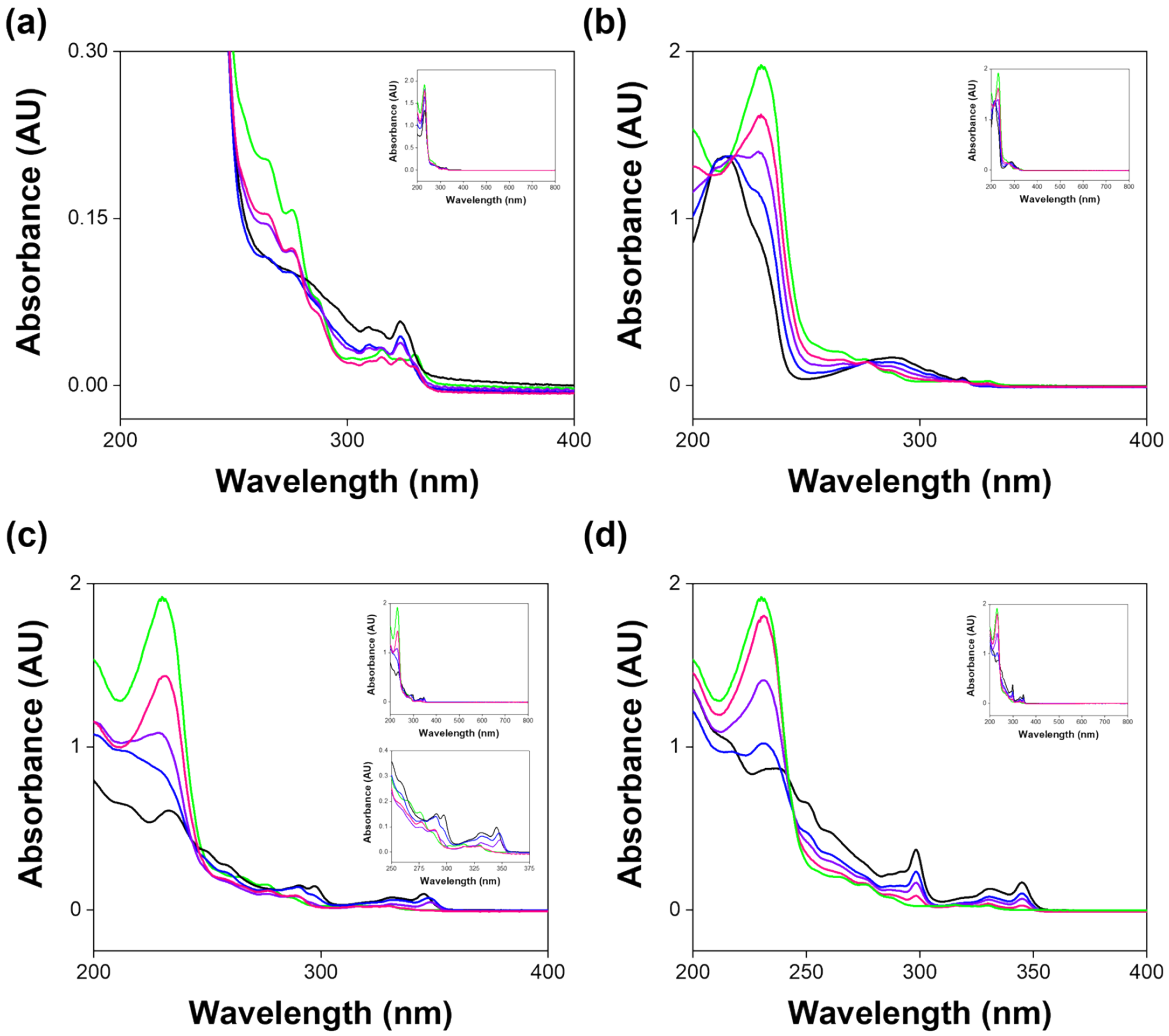

Figure S4. UV-Vis absorption spectra recorded from single and multicomponent systems of (a) 7MeO2NapFV, (b) 1NapVV, (c) CarbFV and (d) CarbIF at concentration ratios second component:2Nap-(*RS*)-FF (mg/mL:mg/mL) of 10:0 (black), 7.5:2.5 (blue), 5:5 (purple) and 2.5:7.5 (pink) collected in H_2O at pH 10.5. The data recorded from 2Nap-(*RS*)-FF 10 mg/mL (green) is shown in each spectrum for easy comparison with the multicomponent systems. The inserts show the entire spectrum (top) and selected regions to make them more visible (bottom).

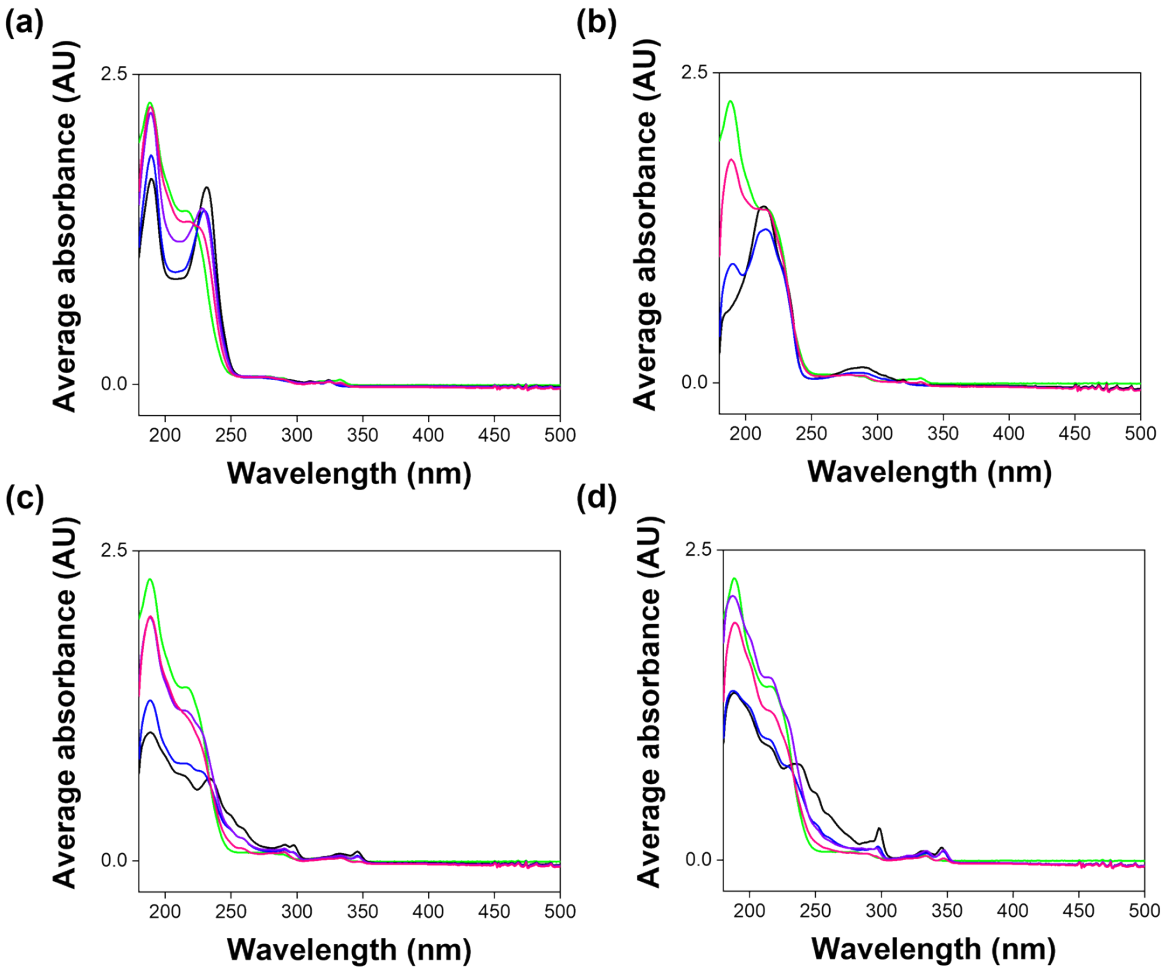

Figure S5. Absorbance spectra recorded concurrently with CD spectra of single and multicomponent systems of (a) 7MeO2NapFV, (b) 1NapVV, (c) CarbFV and (d) CarbIF at concentration ratios second component:2Nap-(*SS*)-FF 10 mg/mL:0 mg/mL (black), 7.5 mg/mL:2.5 mg/mL (blue), 5 mg/mL:5 mg/mL (purple) and 2.5 mg/mL:7.5 mg/mL (pink) at pH 10.5. The spectrum recorded from 2Nap-(*SS*)-FF 10 mg/mL (green) is shown in each spectrum for easy comparison with the multicomponent systems. All data was collected in triplicate and averaged.

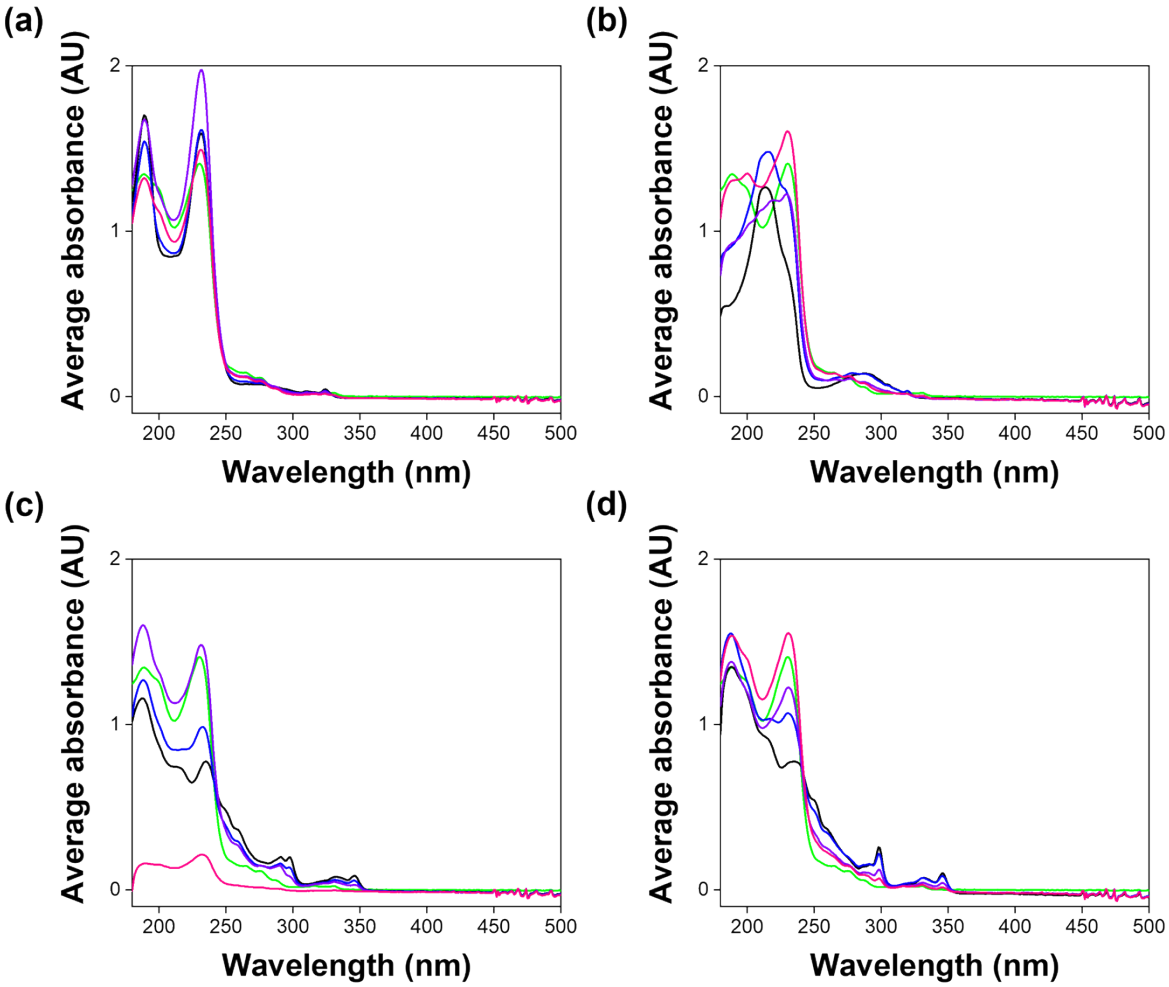

Figure S6. Absorbance spectra recorded concurrently with CD spectra of single and multicomponent systems of (a) 7MeO2NapFV, (b) 1NapVV, (c) CarbFV and (d) CarbIF at concentration ratios second component:2Nap-(*RS*)-FF 10 mg/mL:0 mg/mL (black), 7.5 mg/mL:2.5 mg/mL (blue), 5 mg/mL:5 mg/mL (purple) and 2.5 mg/mL:7.5 mg/mL (pink) at pH 10.5. The spectrum recorded from 2Nap-(*RS*)-FF 10 mg/mL (green) is shown in each spectrum for easy comparison with the multicomponent systems. All data was collected in triplicate and averaged.

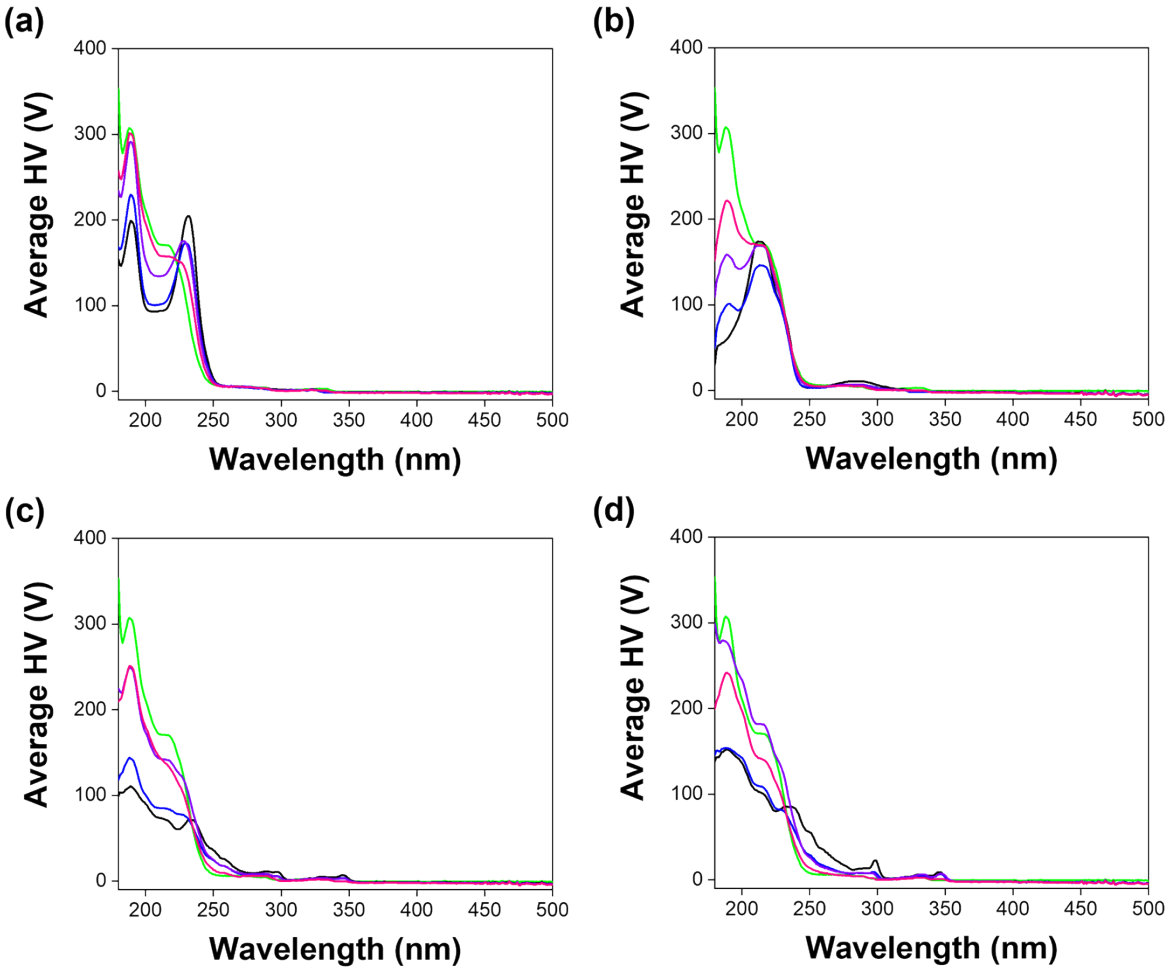

Figure S7. HV spectra recorded concurrently with CD spectra of single and multicomponent systems of (a) 7MeO2NapFV, (b) 1NapVV, (c) CarbFV and (d) CarbIF at concentration ratios second component:2Nap-(*SS*)-FF 10 mg/mL:0 mg/mL (black), 7.5 mg/mL:2.5 mg/mL (blue), 5 mg/mL:5 mg/mL (purple) and 2.5 mg/mL:7.5 mg/mL (pink) at pH 10.5. The spectrum recorded from 2Nap-(*SS*)-FF 10 mg/mL (green) is shown in each spectrum for easy comparison with the multicomponent systems. All data was collected in triplicate and averaged.

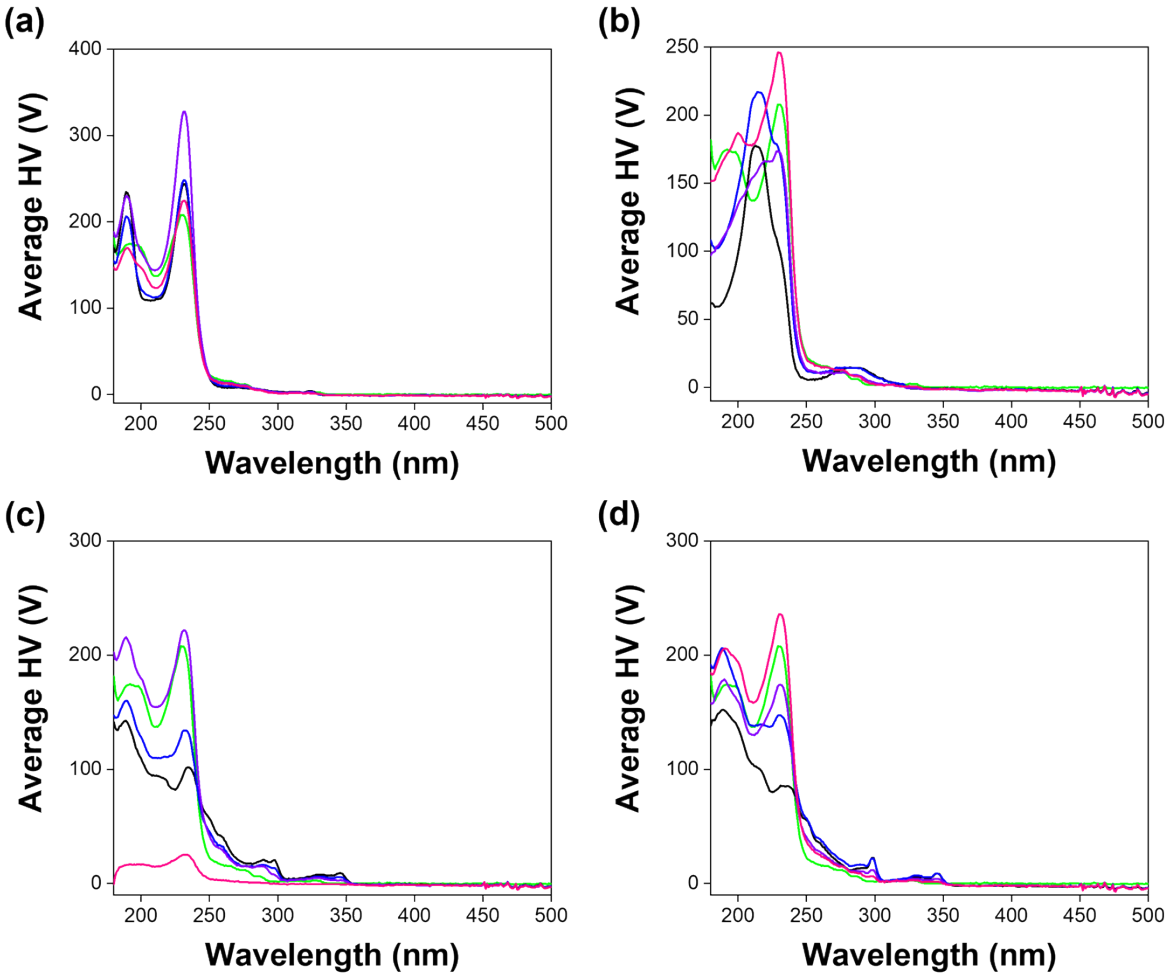

Figure S8. HV spectra recorded concurrently with CD spectra of single and multicomponent systems of (a) 7MeO2NapFV, (b) 1NapVV, (c) CarbFV and (d) CarbIF at concentration ratios second component:2Nap-(*RS*)-FF 10 mg/mL:0 mg/mL (black), 7.5 mg/mL:2.5 mg/mL (blue), 5 mg/mL:5 mg/mL (purple) and 2.5 mg/mL:7.5 mg/mL (pink) at pH 10.5. The spectrum recorded from 2Nap-(*RS*)-FF 10 mg/mL (green) is shown in each spectrum for easy comparison with the multicomponent systems. All data was collected in triplicate and averaged.

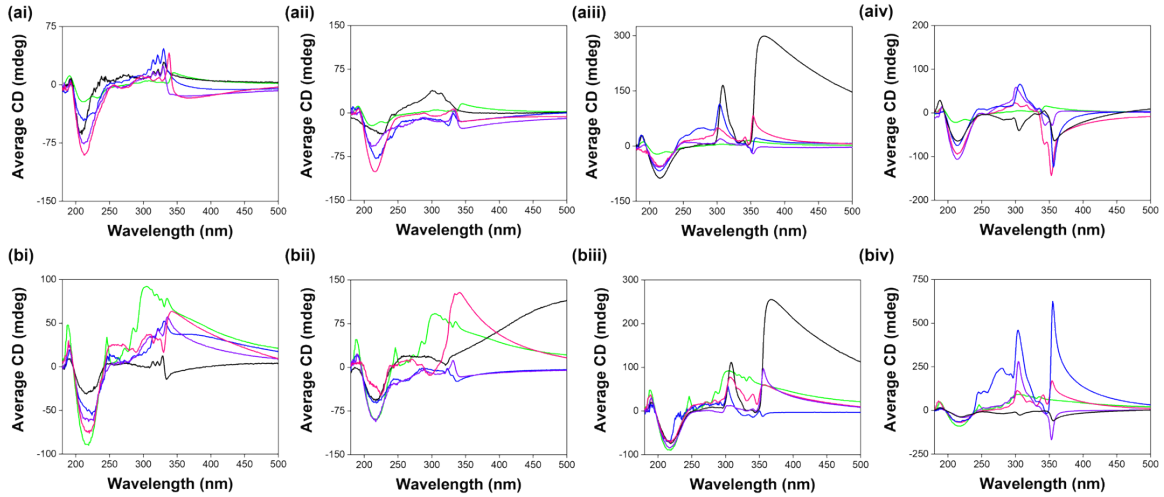

Figure S9. CD spectra recorded from single and multicomponent systems of (i) 7MeO2NapFV, (ii) 1NapVV, (iii) CarbFV and (iv) CarbIF at concentration ratios second component: (a) 2Nap-(*SS*)-FF and (b) 2Nap-(*RS*)-FF of 10 mg/mL:0 mg/mL (black), 7.5 mg/mL:2.5 mg/mL (blue), 5 mg/mL:5 mg/mL (purple) and 2.5 mg/mL:7.5 mg/mL (pink) at low pH in the gel state. The CD spectrum recorded from 2Nap-(*SS*)-FF 10 mg/mL (green) is shown in each spectrum for easy comparison with the multicomponent systems. All data was collected in triplicate and averaged.

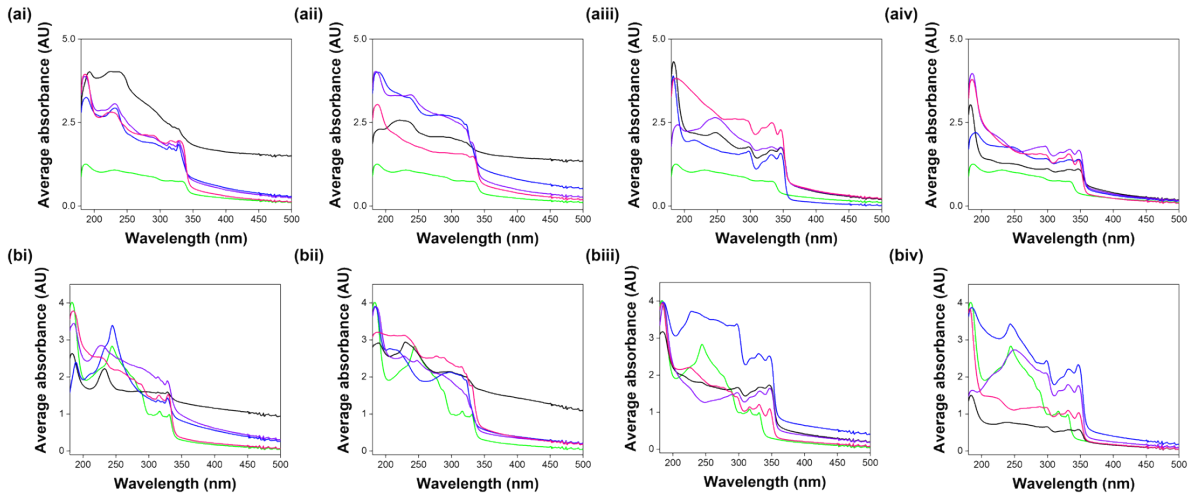

Figure S10. Absorbance spectra recorded concurrently with CD spectra of single and multicomponent systems of (i) 7MeO2NapFV, (ii) 1NapVV, (iii) CarbFV and (iv) CarbIF at concentration ratios second component: (a) 2Nap-(*SS*)-FF and (b) 2Nap-(*RS*)-FF of 10 mg/mL:0 mg/mL (black), 7.5 mg/mL:2.5 mg/mL (blue), 5 mg/mL:5 mg/mL (purple) and 2.5 mg/mL:7.5 mg/mL (pink) in the gel state at low pH. The spectrum recorded from 2Nap-(*SS*)-FF 10 mg/mL (green) is shown in each spectrum for easy comparison with the multicomponent systems. All data was collected in triplicate and averaged.

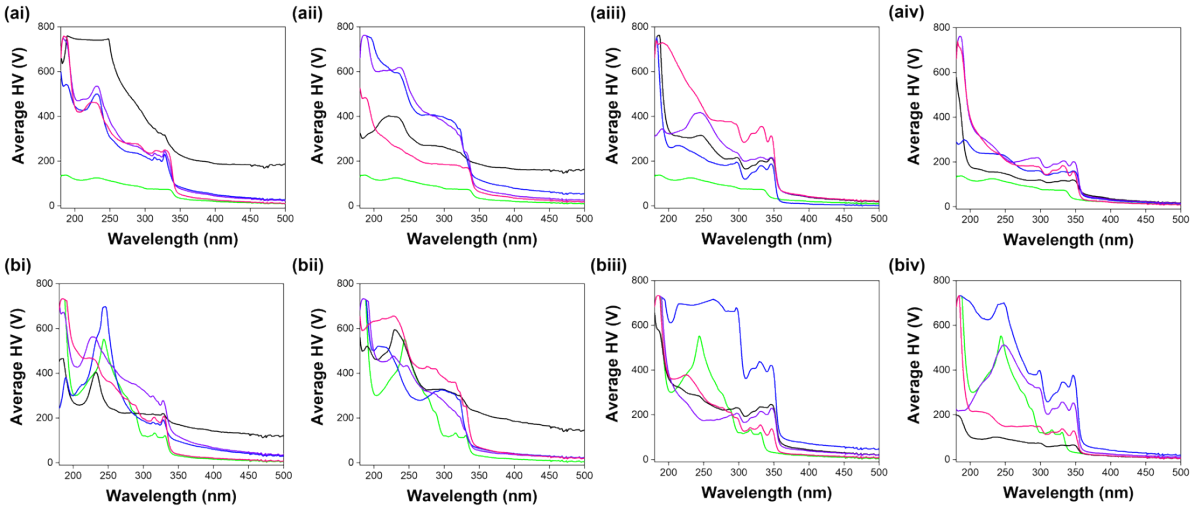

Figure S11. HV spectra recorded concurrently with CD spectra of single and multicomponent systems of (i) 7MeO2NapFV, (ii) 1NapVV, (iii) CarbFV and (iv) CarbIF at concentration ratios second component: (a)2Nap-(*SS*)-FF and (b) 2Nap-(*RS*)-FF of 10 mg/mL:0 mg/mL (black), 7.5 mg/mL:2.5 mg/mL (blue), 5 mg/mL:5 mg/mL (purple) and 2.5 mg/mL:7.5 mg/mL (pink) in the gel state at low pH. The spectrum recorded from 2Nap-(*SS*)-FF 10 mg/mL (green) is shown in each spectrum for easy comparison with the multicomponent systems. All data was collected in triplicate and averaged.

Sample	2Nap-(*SS*)-FF 10 mg/mL	7MeO2NapFV 10 mg/mL	7MeO2NapFV:2 Nap-(*SS*)-FF 5:5 mg/mL	1NapVV 10 mg/mL	1NapVV: 2Nap-(*SS*)-FF 5:5 mg/mL
Model	Hollow cylinder	Elliptical cylinder + power law	Hollow cylinder + power law	Power law	Hollow cylinder + power law
Background	0.018	0.067	0.028	0.072	0.025
A scale	0.0049	3.32×10^{-4}	0.0017	5.79×10^{-8}	0.0019
A scale error	*4.46×10^{-5}*	*2.47×10^{-6}*	*6.03×10^{-5}*	*5.32×10^{-9}*	*5.93×10^{-5}*
A radius	18.0	141.6	18.4	-	18.6
A radius error	*0.11*	*1.0*	*0.43*	-	*0.33*
A radius polydispersity	0.1	0.3	-	-	-
A thickness	17.7	-	17.6	-	16.6
A thickness error	*0.18*	-	*0.73*	-	*0.58*
A axis ratio	-	1.99	-	-	-
A axis ratio error	-	*0.06*	-	-	-
A length	5000	745.8	744.5	-	5000
A length error	-	*4.39*	*98.7*	-	-
B scale	-	0.0016	7.07×10^{-4}	-	7.86×10^{-5}
B scale error	-	*6.97×10^{-5}*	*7.41×10^{-5}*	-	*1.37×10^{-5}*
B power	-	0.93	1.45	3.64	1.86
B power error	-	*0.017*	*0.035*	*0.020*	*0.042*
Reduced chi2	**10.68**	**23.63**	**1.08**	**9.04**	**1.36**

SANS fitting parameters

Table S2. Summary of the parameters obtained from fitting SANS data collected at high pH. Fitting parameters obtained from SasView model fitting of the SANS data. Parameter errors are fitting errors.

Sample	2Nap-(*RS*)-FF 10 mg/mL	7MeO2NapFV 10 mg/mL	7MeO2NapFV:2 Nap-(*RS*)-FF 5:5 mg/mL	1NapVV 10 mg/mL	1NapVV: 2Nap-(*RS*)-FF 5:5 mg/mL
Model	Hollow cylinder	Elliptical cylinder + power law	Hollow cylinder + power law	Power law	Hollow cylinder + power law
Background	0.065	0.067	0.060	0.072	0.063
A scale	0.0042	3.32×10^{-4}	0.0022	5.79×10^{-8}	0.0049
A scale error	*6.27×10^{-5}*	*2.47×10^{-6}*	*1.04×10^{-5}*	*5.32×10^{-9}*	*2.08×10^{-4}*
A radius	128.3	141.6	128.8	-	130.4
A radius error	*0.12*	*1.0*	-	-	*0.18*
A radius polydispersity	-	0.3	0.05	-	0.05
A thickness	14.1	-	14.1	-	7.9
A thickness error	*0.22*	-	-	-	*0.35*
A axis ratio	-	1.99	-	-	-
A axis ratio error	-	*0.06*	-	-	-
A length	555.2	745.8	555.2	-	539.3
A length error	*4.20*	*4.39*	-	-	*4.29*
B scale	-	0.0016	1.73×10^{-5}	-	4.09×10^{-9}
B scale error	-	*6.97×10^{-5}*	*2.805×10^{-7}*	-	*1.52×10^{-10}*
B power	-	0.93	2.4	3.64	4.1
B power error	-	*0.017*	-	*0.020*	-
Reduced chi2	**22.09**	**23.63**	**49.30**	**9.04**	**14.53**

Table S3. Summary of the parameters obtained from fitting SANS data collected at high pH. Fitting parameters obtained from SasView model fitting of the SANS data. Parameter errors are fitting errors.

Sample	2Nap-(*SS*)-FF 10 mg/mL	CarbFV 10 mg/mL	CarbFV: 2Nap-(*SS*)-FF 5:5 mg/mL	CarbFV: 2Nap-(*SS*)-FF 5:5 mg/mL	CarbIF 10 mg/mL	CarbIF: 2Nap-(*SS*)-FF 5:5 mg/mL	CarbIF: 2Nap-(*SS*)-FF 5:5 mg/mL
Model	Hollow cylinder	Hollow cylinder + power law	Hollow cylinder + power law	Hollow cylinder + hollow cylinder	Hollow cylinder + power law	Hollow cylinder	Hollow cylinder + flexible cylinder
Background	0.018	0.063	0.016	0.019	0.068	0.026	0.026
A scale	0.0049	0.0022	0.0031	0.0016	0.0069	0.0049	*0.0042*
A scale error	*4.46 x10^{-5}*	*1.88 x10^{-5}*	*2.38 x10^{-5}*	*1.97 x10^{-4}*	*2.60 x10^{-5}*	*4.24 x10^{-5}*	*9.26 x10^{-5}*
A radius	18.0	18.7	17.6	10.9	23.1	11.8	13.5
A radius error	*0.11*	*0.16*	*0.15*	*1.82*	*0.047*	*0.13*	*0.27*
A radius polydispersity	0.1	-	-	-	-	0.2	-
A thickness	17.7	29.5	28.3	21.5	20.9	19.2	17.7
A thickness error	*0.18*	*0.26*	*0.24*	*7.32*	*0.081*	*0.20*	*0.37*
A length	5000	161.9	290.6	5000	363.0	5000	5000
A length error	-	*1.37*	*4.07*	-	*2.89*	-	-
B scale	-	4.45 x10^{-4}	2.72 x10^{-4}	0.0032	5.443 x10^{-6}	-	6.62 x10^{-4}
B scale error	-	*5.97 x10^{-6}*	*1.13 x10^{-5}*	*1.35 x10^{-4}*	*8.42 x10^{-7}*	-	*3.66 x10^{-5}*
B radius	-	-	-	24.1	-	-	26.6
B radius error	-	-	-	*3.17*	-	-	*0.47*
B thickness	-	-	-	20.2	-	-	-
B thickness error	-	-	-	*3.47*	-	-	-
B length	-	-	-	1088.7	-	-	61.8
B length error	-	-	-	*3.47*	-	-	*0.0018*
B power	-	2.09	1.94	-	2.70	-	618.3
B power error	-	*0.0039*	*0.013*	-	*0.034*	-	*33.54*
Reduced chi2	**10.68**	**5.98**	**1.83**	**2.96**	**31.04**	**6.16**	**2.24**

Table S4. Summary of the parameters obtained from fitting SANS data collected at high pH. Fitting parameters obtained from SasView model fitting of the SANS data. Parameter errors are fitting errors.

Sample	2Nap-(*RS*)-FF 10 mg/mL	CarbFV 10 mg/mL	CarbFV: 2Nap-(*RS*)-FF 5:5 mg/mL	CarbIF 10 mg/mL	CarbIF: 2Nap-(*RS*)-FF 5:5 mg/mL
Model	Hollow cylinder	Hollow cylinder + power law	Hollow cylinder + hollow cylinder	Hollow cylinder + power law	Hollow cylinder + hollow cylinder
Background	0.065	0.063	0.058	0.068	0.061
A scale	0.0042	0.0022	0.030	0.0069	0.0020
A scale error	*6.27 x10^{-5}*	*1.88 x10^{-5}*	*5.61 x10^{-5}*	*2.60 x10^{-5}*	*5.71 x10^{-5}*
A radius	128.3	18.7	127.6	23.1	127.7
A radius error	*0.12*	*0.16*	*0.16*	*0.047*	*0.25*
A thickness	14.1	29.5	13.2	20.9	14.7
A thickness error	*0.22*	*0.26*	*0.27*	*0.081*	*0.48*
A length	555.2	161.9	463.7	363.0	448.3
A length error	*4.20*	*1.37*	*4.72*	*2.89*	*6.48*
B scale	-	4.45 x10^{-4}	0.0026	5.443 x10^{-6}	0.0030
B scale error	-	*5.97 x10^{-6}*	*3.457 x10^{-5}*	*8.42 x10^{-7}*	*5.84 x10^{-5}*
B radius	-	-	23.8	-	26.7
B radius error	-	-	*0.15*	-	*0.16*
B thickness	-	-	13.2	-	13.9
B thickness error	-	-	*0.27*	-	*0.29*
B length	-	-	261.2	-	552.8
B length error	-	-	*5.43*		*15.70*
B power	-	2.09	-	2.70	-
B power error	-	*0.0039*	-	*0.034*	-
Reduced chi2	**22.09**	**5.98**	**202.45**	**31.04**	**55.75**

Table S5. Summary of the parameters obtained from fitting SANS data collected at high pH. Fitting parameters obtained from SasView model fitting of the SANS data. Parameter errors are fitting errors.

Sample	2Nap-(*SS*)-FF 10 mg/mL	7MeO2NapFV 10 mg/mL	7MeO2NapFV:2 Nap-(*SS*)-FF 5:5 mg/mL	1NapVV 10 mg/mL	1NapVV: 2Nap-(*SS*)-FF 5:5 mg/mL
Model	Hollow cylinder	Elliptical cylinder + power law	Hollow cylinder + power law	Power law	Hollow cylinder + power law
Background	0.018	0.067	0.028	0.072	0.025
A scale	0.0049	3.32×10^{-4}	0.0017	5.79×10^{-8}	0.0019
A scale error	*4.46×10^{-5}*	*2.47×10^{-6}*	*6.03×10^{-5}*	*5.32×10^{-9}*	*5.93×10^{-5}*
A radius	18.0	141.6	18.4	-	18.6
A radius error	*0.11*	*1.00*	*0.43*	-	*0.33*
A radius polydispersity	0.1	0.3	-	-	-
A thickness	17.7	-	17.6	-	16.6
A thickness error	*0.18*	-	*0.73*	-	*0.58*
A axis ratio	-	1.99	-	-	-
A axis ratio error	-	*0.06*	-	-	-
A length	5000	745.8	744.5	-	5000
A length error	-	*4.39*	*98.7*	-	-
B scale	-	0.0016	7.07×10^{-4}	-	7.86×10^{-5}
B scale error	-	*6.97×10^{-5}*	*7.41×10^{-5}*	-	*1.37×10^{-5}*
B power	-	0.93	1.45	3.64	1.86
B power error	-	*0.017*	*0.035*	*0.020*	*0.042*
Reduced chi2	**10.68**	**23.63**	**1.08**	**9.04**	**1.36**

Table S6. Summary of the parameters obtained from fitting SANS data collected at low pH. Fitting parameters obtained from SasView model fitting of the SANS data. Parameter errors are fitting errors.

Sample	2Nap-(*RS*)-FF 10 mg/mL	7MeO2NapFV 10 mg/mL	7MeO2NapFV: 2Nap-(*RS*)-FF 5:5 mg/mL	1NapVV 10 mg/mL	1NapVV: 2Nap-(*RS*)-FF 5:5 mg/mL
Model	Hollow cylinder	Flexible elliptical cylinder	Hollow cylinder + power law	Flexible elliptical cylinder	Flexible elliptical cylinder
Background	0.092	0.081	0.065	0.068	0.069
A scale	0.0035	5.05×10^{-4}	4.81×10^{-4}	0.0025	0.0035
A scale error	*2.02×10^{-5}*	*2.10×10^{-5}*	*7.30×10^{-6}*	*2.93×10^{-5}*	*1.88×10^{-5}*
A radius	125.1	60.3	106.8	177.9	37.8
A radius error	*0.11*	*0.73*	*0.61*	*0.68*	*0.082*
A radius polydispersity	-	0.5	-	0.3	0.2
A thickness	25.3	-	64.4	-	-
A thickness error	*0.17*	-	*0.95*	-	-
A axis ratio	-	3.78	-	1.67	-
A axis ratio error	-	*0.11*	-	*0.018*	-
A Kuhn length	-	132.08	-	422.33	376.83
A Kuhn length error	-	*4.83*	-	*7.50*	*0.082*
A length	575.2	5000	494.2	5000	815.2
A length error	*4.07*	-	*12.58*	-	*15.28*
B scale	-	-	-	-	-
B scale error	-	-	-	-	-
B power	-	-	-	-	-
B power error	-	-	-	-	-
Reduced chi2	**61.07**	**6.55**	**9.98**	**10.01**	**12.37**

Table S7. Summary of the parameters obtained from fitting SANS data collected at low pH. Fitting parameters obtained from SasView model fitting of the SANS data. Parameter errors are fitting errors.

Sample	2Nap-(*SS*)-FF 10 mg/mL	CarbFV 10 mg/mL	CarbFV: 2Nap-(*SS*)-FF 5:5 mg/mL	CarbIF 10 mg/mL	CarbIF: 2Nap-(*SS*)-FF 5:5 mg/mL
Model	Flexible elliptical cylinder + power law	Flexible cylinder + power law	Elliptical cylinder + power law	Flexible cylinder + power law	Flexible cylinder + power law
Background	0.022	0.071	0.025	0.079	0.025
A scale	3.31 x10^{-4}	0.0020	0.0036	0.0029	0.0019
A scale error	*1.15 x10^{-5}*	*3.45 x10^{-5}*	*1.89 x10^{-5}*	*3.21 x10^{-5}*	*9.62* x10^{-5}
A radius	22.5	52.7	34.7	48.5	38.9
A radius error	*0.35*	*0.017*	*0.25*	*0.13*	*0.19*
A radius polydispersity	0.15	-	0.1	-	-
A axis ratio	3.42	-	1.43	-	-
A axis ratio error	*0.060*	-	*0.020*	-	-
A Kuhn length	15.6	84.8	-	80.2	39.9
A Kuhn length error	*0.62*	*2.95*	-	*1.81*	*3.40*
A length	5000	5000	5000	3370.8	909.5
A length error	-	-	-	*90.99*	*51.98*
B scale	2.043 x10^{-5}	2.68 x10^{-4}	7.76 x10^{-5}	7.95 x10^{-4}	5.58 x10^{-5}
B scale error	*2.84 x10^{-6}*	*1.04 x10^{-5}*	*4.09 x10^{-6}*	*4.14 x10^{-5}*	*1.86 x10^{-6}*
B power	2.75	2.09	2.31	1.66	2.59
B power error	*0.027*	*0.015*	*0.011*	*0.0023*	*0.0070*
Reduced chi2	**12.81**	**19.74**	**3.54**	**21.77**	**8.56**

Table S8. Summary of the parameters obtained from fitting SANS data collected at low pH. Fitting parameters obtained from SasView model fitting of the SANS data. Parameter errors are fitting errors.

Sample	2Nap-(*RS*)-FF 10 mg/mL	CarbFV 10 mg/mL	CarbFV: 2Nap-(*RS*)-FF 5:5 mg/mL	CarbIF 10 mg/mL	CarbIF: 2Nap-(*RS*)-FF 5:5 mg/mL
Model	Hollow cylinder	Flexible cylinder + power law	Elliptical cylinder + power law	Flexible cylinder + power law	Flexible cylinder + power law
Background	0.092	0.071	0.066	0.079	0.070
A scale	0.0035	0.0020	0.0027	0.0029	0.0026
A scale error	*2.02 x10^{-5}*	*3.45 x10^{-5}*	*1.35 x10^{-5}*	*3.21 x10^{-5}*	*1.36 x10^{-5}*
A radius	125.1	52.7	45.1	48.5	58.8
A radius error	*0.11*	*0.017*	*0.11*	*0.13*	*0.08*
A radius polydispersity	-	-	-	-	-
A thickness	25.3	-	-	-	-
A thickness error	*0.17*	-	-	-	-
A axis ratio	-	-	1.56	-	-
A axis ratio error	-	-	*0.013*	-	-
A Kuhn length	-	84.81	81.0	80.18	176.7
A Kuhn length error	-	*2.95*	*2.51*	*1.81*	*0.0015*
A length	575.2	5000	5000	3370.8	706.9
A length error	*4.07*	-	-	*90.99*	*23.8*
B scale	-	2.68 x10^{-4}	8.43 x10^{-5}	7.95 x10^{-4}	9.44 x10^{-5}
B scale error	-	*1.04 x10^{-5}*	*1.39 x10^{-6}*	*4.14 x10^{-5}*	*4.08 x10^{-5}*
B power	-	2.09	2.60	1.66	2.41
B power error	-	*0.015*	*0.0042*	*0.0023*	*0.017*
Reduced chi2	**61.07**	**19.74**	**25.00**	**21.77**	**10.05**

Table S9. Summary of the parameters obtained from fitting SANS data collected at low pH. Fitting parameters obtained from SasView model fitting of the SANS data. Parameter errors are fitting errors.

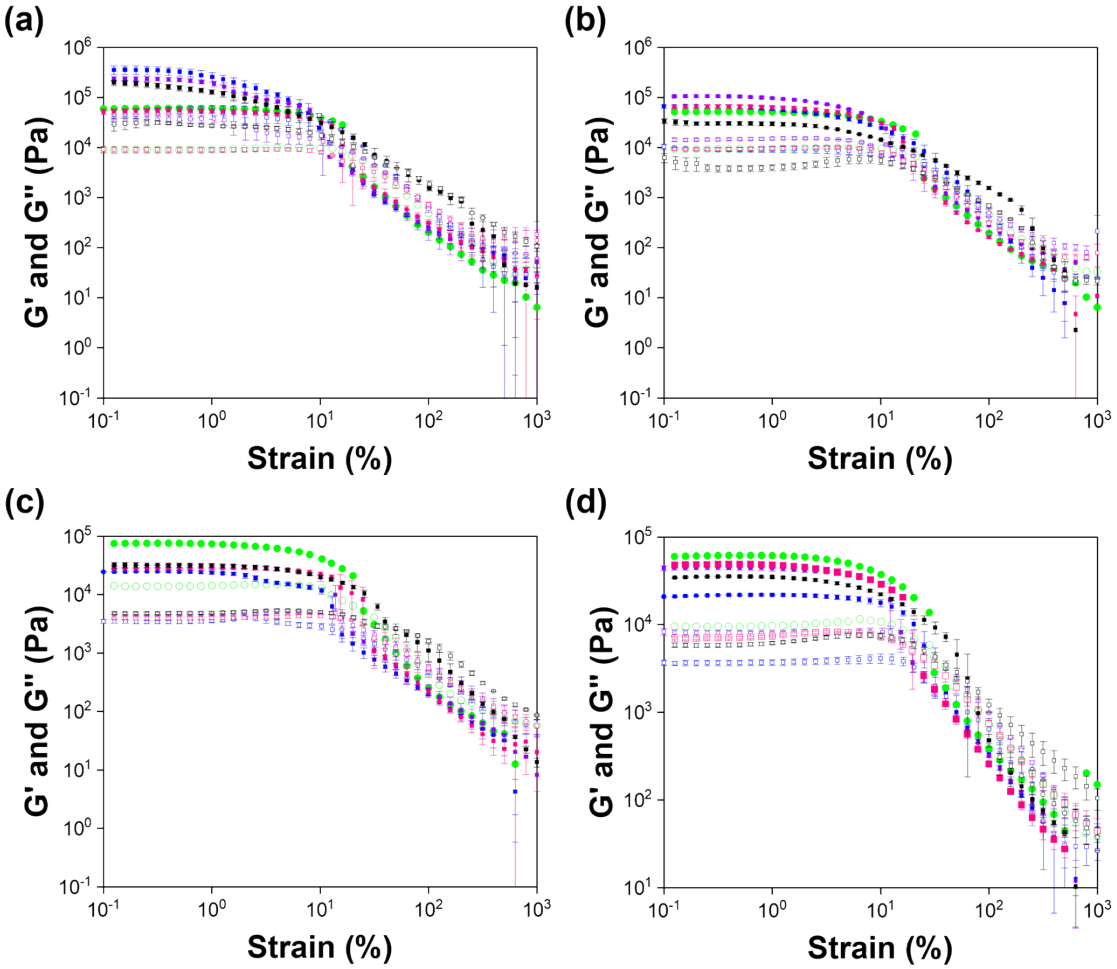

Figure S12. Full strain sweeps recorded from gels composed of single and multicomponent systems of (i) 7MeO2NapFV, (ii) 1NapVV, (iii) CarbFV and (iv) CarbIF at concentration ratios second component:2Nap-(*SS*)-FF of 10 mg/mL:0 mg/mL (black), 7.5 mg/mL:2.5 mg/mL (blue), 5 mg/mL:5 mg/mL (purple) and 2.5 mg/mL:7.5 mg/mL (pink) in the gel state at low pH. The strain sweep data recorded from 2Nap-(*SS*)-FF 10 mg/mL (green) are shown in each strain sweep for easy comparison with the multicomponent systems. All data was collected in triplicate and averaged. The error bars show the standard deviation between samples.

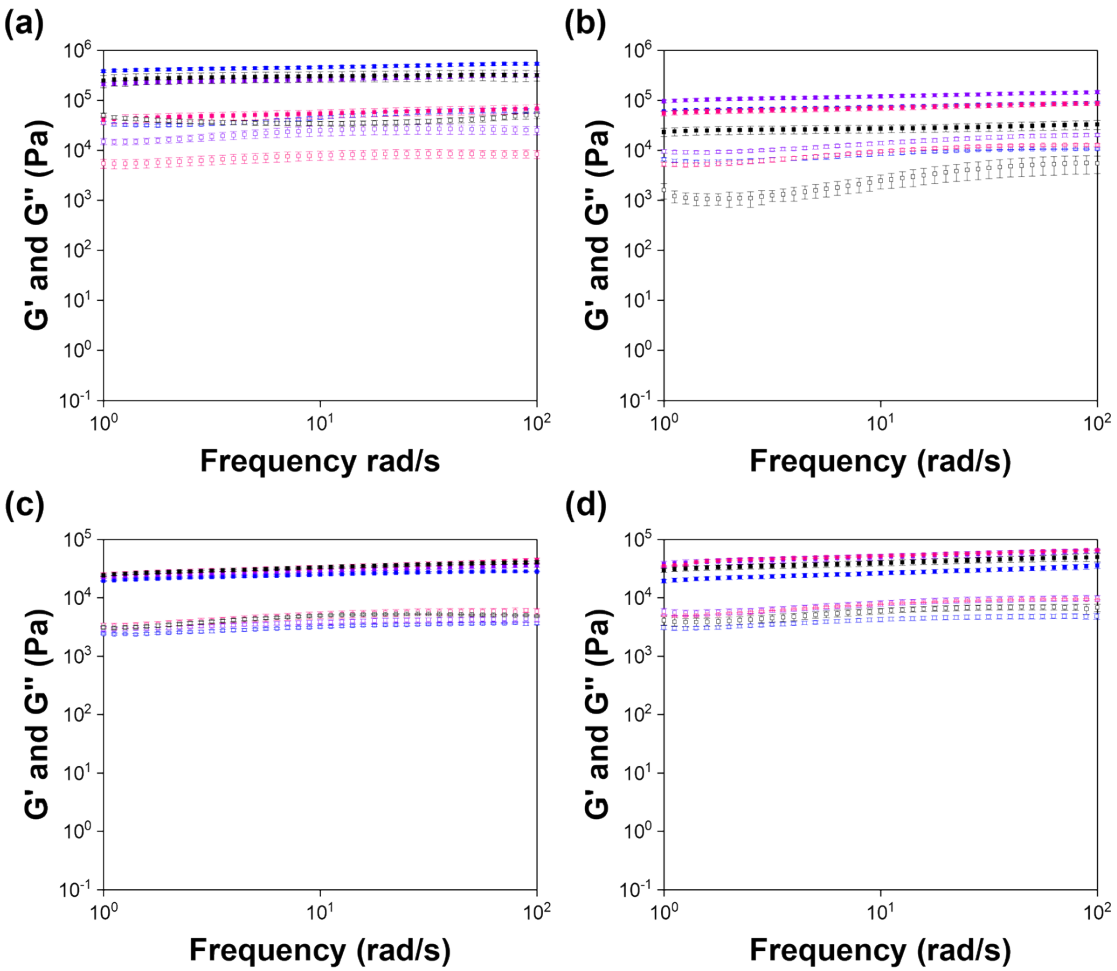

Figure S13. Full frequency sweeps recorded from gels composed of single and multicomponent systems of (i) 7MeO2NapFV, (ii) 1NapVV, (iii) CarbFV and (iv) CarbIF at concentration ratios second component:2Nap-(*SS*)-FF of 10 mg/mL:0 mg/mL (black), 7.5 mg/mL:2.5 mg/mL (blue), 5 mg/mL:5 mg/mL (purple) and 2.5 mg/mL:7.5 mg/mL (pink) in the gel state at low pH. The strain sweep data recorded from 2Nap-(*SS*)-FF 10 mg/mL (green) are shown in each strain sweep for easy comparison with the multicomponent systems. All data was collected in triplicate and averaged. The error bars show the standard deviation between samples.

Rheology data

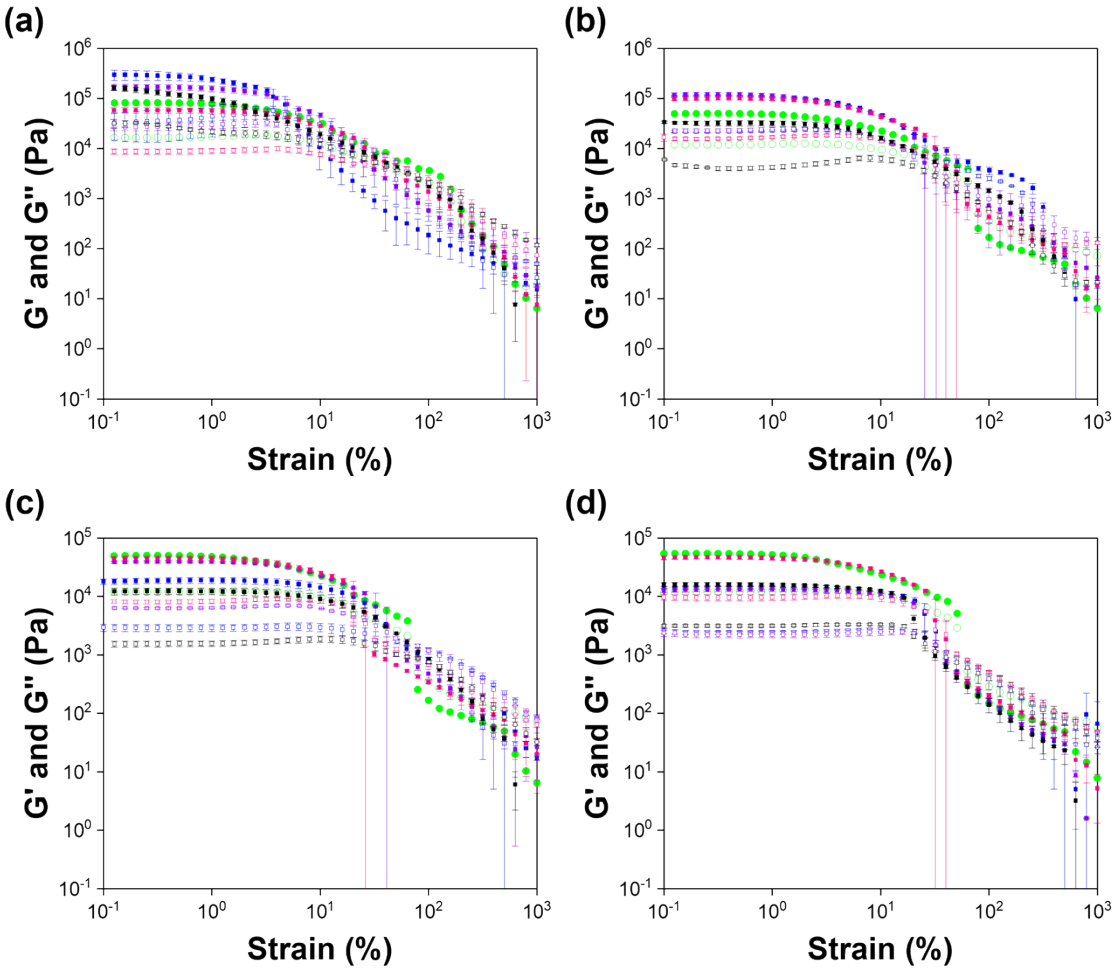

Figure S14. Full strain sweeps recorded from gels composed of single and multicomponent systems of (i) 7MeO2NapFV, (ii) 1NapVV, (iii) CarbFV and (iv) CarbIF at concentration ratios second component:2Nap-(*RS*)-FF of 10 mg/mL:0 mg/mL (black), 7.5 mg/mL:2.5 mg/mL (blue), 5 mg/mL:5 mg/mL (purple) and 2.5 mg/mL:7.5 mg/mL (pink) in the gel state at low pH. The strain sweep data recorded from 2Nap-(*RS*)-FF 10 mg/mL (green) are shown in each strain sweep for easy comparison with the multicomponent systems. All data was collected in triplicate and averaged. The error bars show the standard deviation between samples.

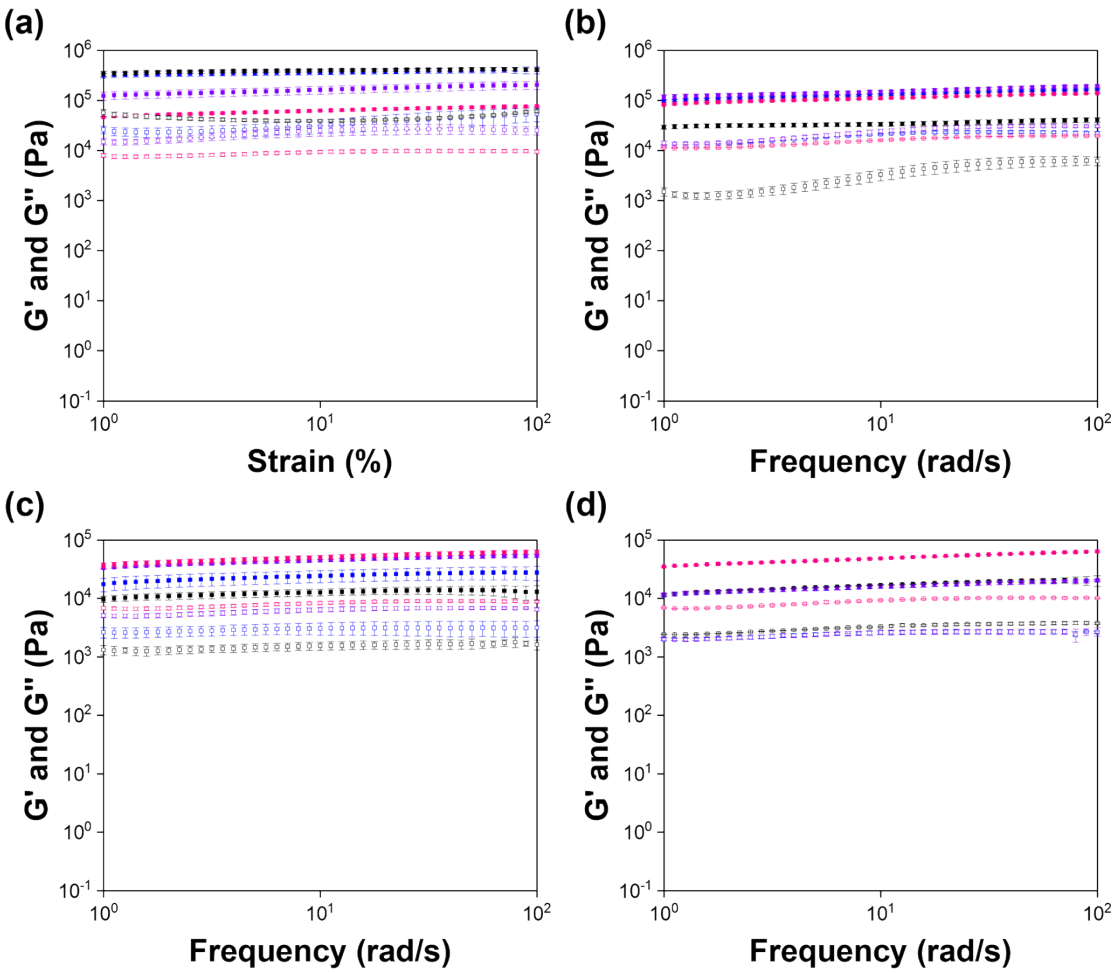

Figure S15. Full frequency sweeps recorded from gels composed of single and multicomponent systems of (i) 7MeO2NapFV, (ii) 1NapVV, (iii) CarbFV and (iv) CarbIF at concentration ratios second component:2Nap-(*RS*)-FF of 10 mg/mL:0 mg/mL (black), 7.5 mg/mL:2.5 mg/mL (blue), 5 mg/mL:5 mg/mL (purple) and 2.5 mg/mL:7.5 mg/mL (pink) in the gel state at low pH. The strain sweep data recorded from 2Nap-(*RS*)-FF 10 mg/mL (green) are shown in each strain sweep for easy comparison with the multicomponent systems. All data was collected in triplicate and averaged. The error bars show the standard deviation between samples.

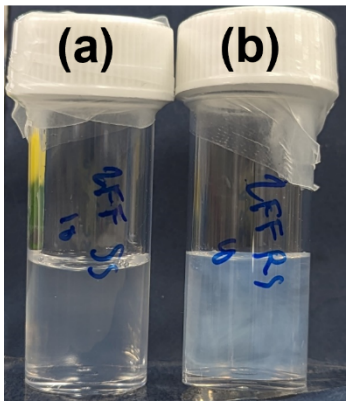

Photographs of solutions and gels

Figure S16. Photographs of solutions (pH 10.5) composed of (a) 2Nap-(*SS*)-FF and (b) 2Nap-(*RS*)-FF at concentrations of 10 mg/mL.

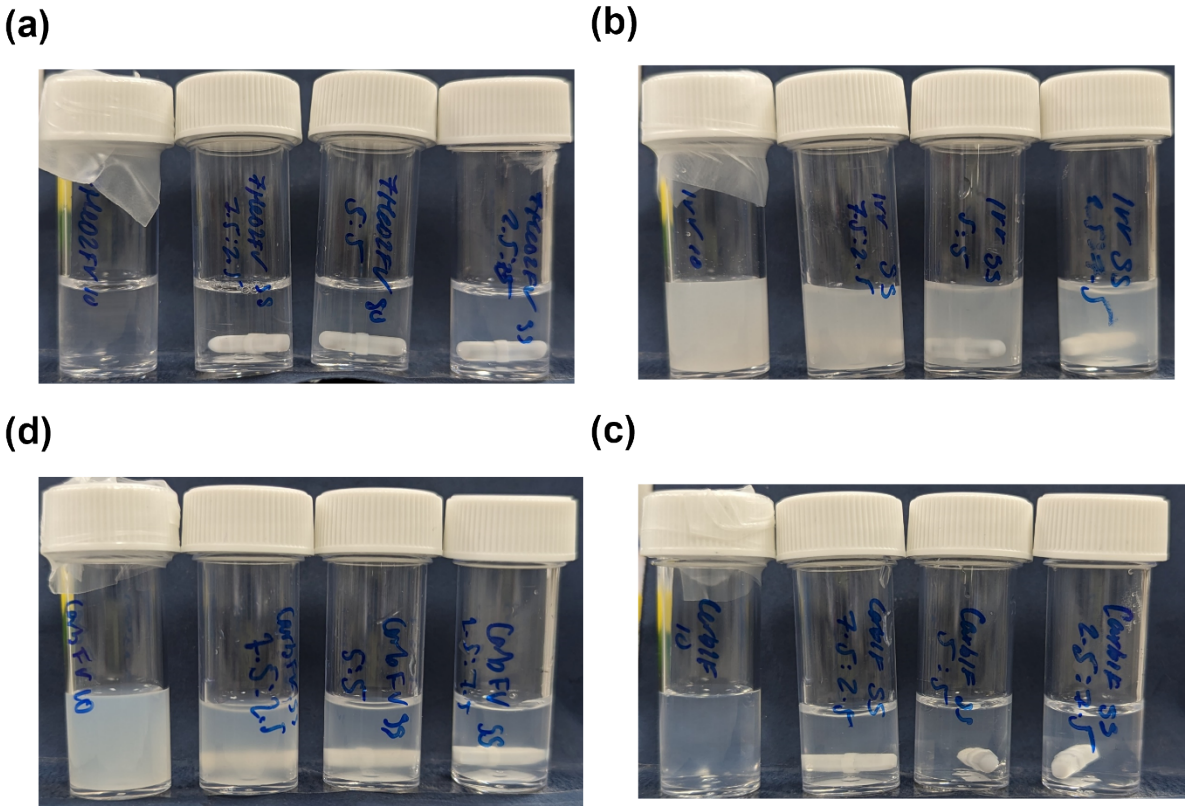

Figure S17. Photographs of solutions (pH 10.5) composed of (a) 1NapVV, (b) 7MeO2NapFV, (c) CarbFV and (d) CarbIF and 2Nap-(*SS*)-FF at concentration ratios of 10 mg/mL:0 mg/mL, 7.5 mg/mL:2.5 mg/mL, 5 mg/mL:5 mg/mL and 2.5 mg/mL (second component:2Nap-(*SS*)-FF, left-to-right.

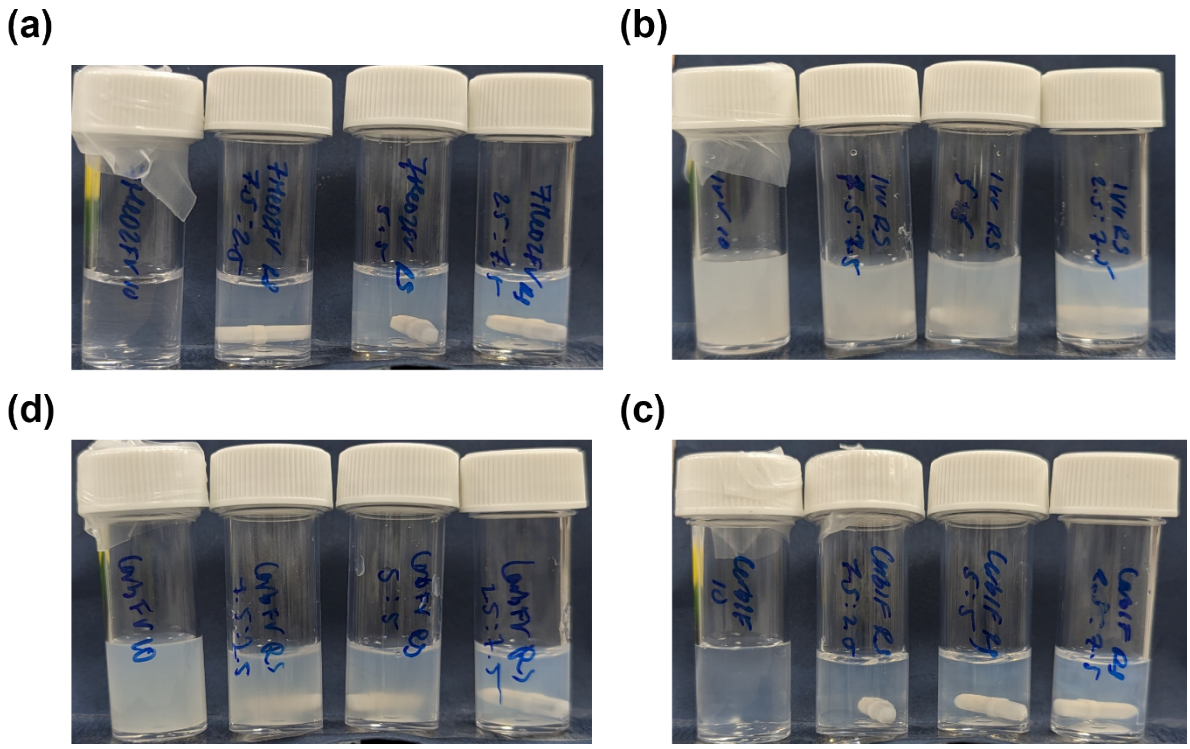

Figure S18. Photographs of solutions (pH 10.5) composed of (a) 1NapVV, (b) 7MeO2NapFV, (c) CarbFV and (d) CarbIF and 2Nap-(*SS*)-FF at concentration ratios of 10 mg/mL:0 mg/mL, 7.5 mg/mL:2.5 mg/mL, 5 mg/mL:5 mg/mL and 2.5 mg/mL (second component:2Nap-(*SS*)-FF, left-to-right.

Figure S19. Photographs of gels (pH 3.5) composed of (a) 2Nap-(*SS*)-FF and (b) 2Nap-(*RS*)-FF at concentrations of 10 mg/mL.

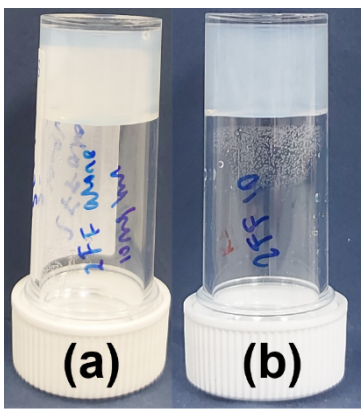

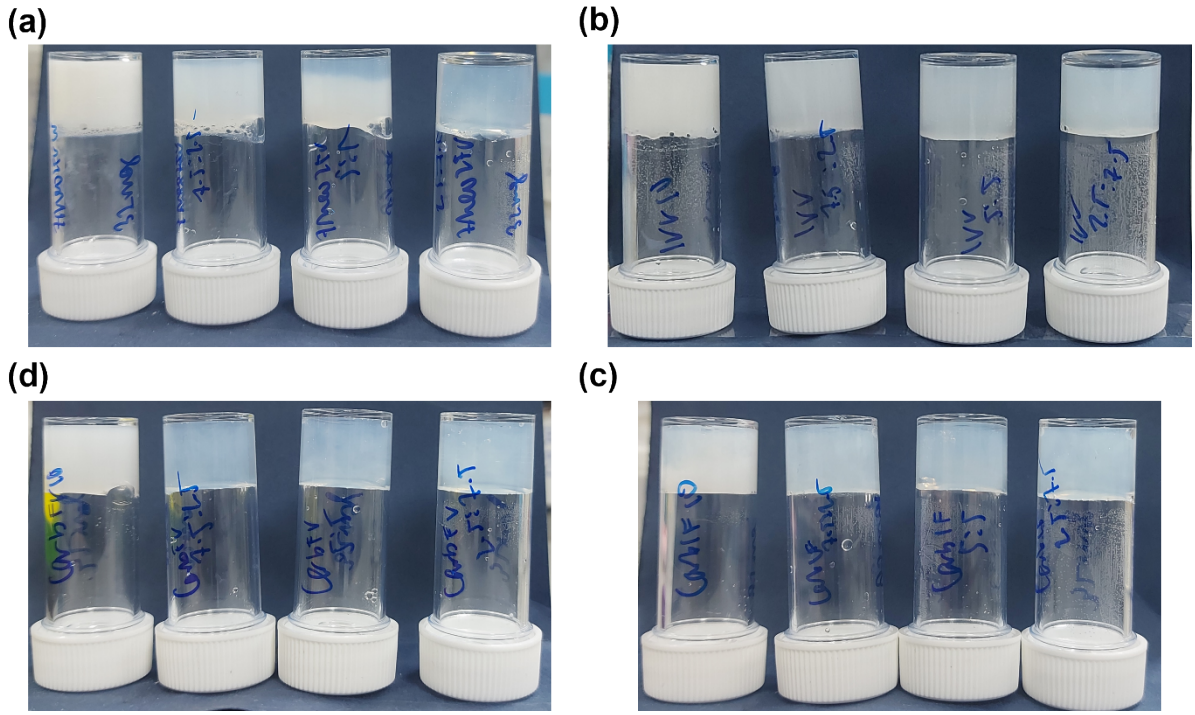

Figure S20. Photographs of gels (pH 3.5) composed of (a) 1NapVV, (b) 7MeO2NapFV, (c) CarbFV and (d) CarbIF and 2Nap-(*SS*)-FF at concentration ratios of 10 mg/mL:0 mg/mL, 7.5 mg/mL:2.5 mg/mL, 5 mg/mL:5 mg/mL and 2.5 mg/mL (second component:2Nap-(*SS*)-FF, left-to-right.

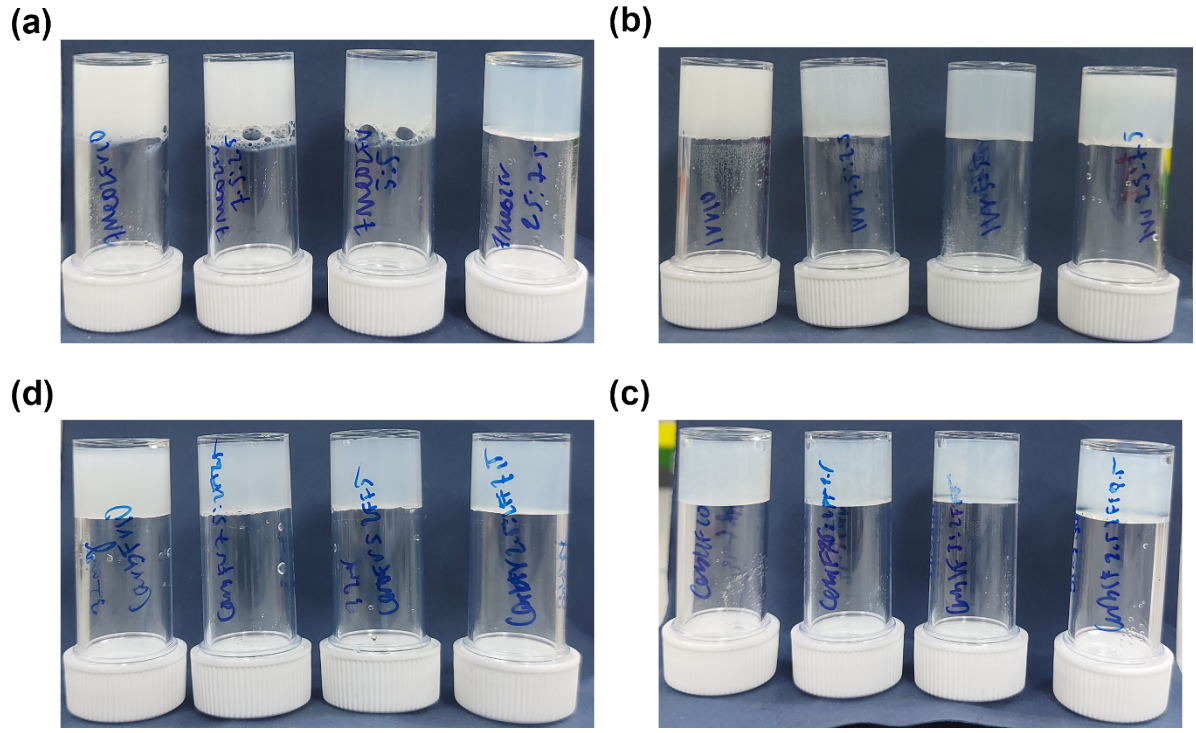

Figure S21. Photographs of gels (pH 3.5) composed of (a) 1NapVV, (b) 7MeO2NapFV, (c) CarbFV and (d) CarbIF and 2Nap-(*RS*)-FF at concentration ratios of 10 mg/mL:0 mg/mL, 7.5 mg/mL:2.5 mg/mL, 5 mg/mL:5 mg/mL and 2.5 mg/mL (second component:2Nap-(*RS*)-FF, left-to-right.

PXRD

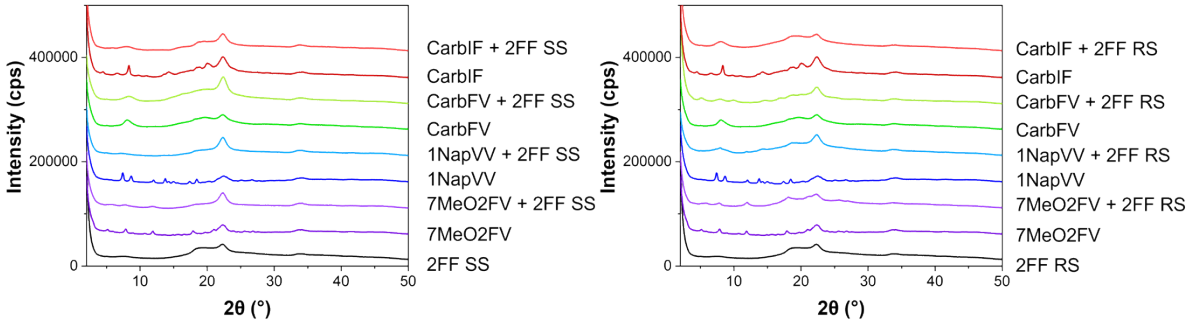

Figure S22. PXRD patterns obtained from each freeze-dried gels composed of each system named on the right-hand side of each plot. All the systems have a total concentration of 10 mg/mL with the multicomponent systems prepared at a concentration ratio of 5 mg/mL:5 mg/mL.

References

1. https://www.ncnr.nist.gov/resources/sldcalc.html.
2. O. Arnold, J. C. Bilheux, J. M. Borreguero, A. Buts, S. I. Campbell, L. Chapon, M. Doucet, N. Draper, R. F. Leal, M. A. Gigg, V. E. Lynch, A. Markvardsen, D. J. Mikkelson, R. L. Mikkelson, R. Miller, K. Palmen, P. Parker, G. Passos, T. G. Perring, P. F. Peterson, S. Ren, M. A. Reuter, A. T. Savici, J. W. Taylor, R. J. Taylor, R. Tolchenoy, W. Zhou and J. Zikoysky, *Nuclear Instruments & Methods in Physics Research Section a-Accelerators Spectrometers Detectors and Associated Equipment*, 2014, **764**, 156-166.
3. https://www.sasview.org.
4. A. Ruter, S. Kuczera, D. J. Pochan and U. Olsson, *Langmuir*, 2019, **35**, 5802-5808.
5. B. O. Okesola, Y. Wu, B. Derkus, S. Gani, D. Wu, D. Knani, D. K. Smith, D. J. Adams and A. Mata, *Chemistry of Materials*, 2019, **31**, 7883-7897.
6. C. Colquhoun, E. R. Draper, E. G. Eden, B. N. Cattoz, K. L. Morris, L. Chen, T. O. McDonald, A. E. Terry, P. C. Griffiths, L. C. Serpell and D. J. Adams, *Nanoscale*, 2014, **6**, 13719-13725.
7. K. McAulay, B. Dietrich, H. Su, M. T. Scott, S. Rogers, Y. K. Al-Hilaly, H. Cui, L. C. Serpell, A. M. Seddon, E. R. Draper and D. J. Adams, *Chemical Science*, 2019, **10**, 7801-7806.
8. E. R. Draper, H. Su, C. Brasnett, Poole, R. J., S. Rogers, H. Cui, A. Sneddon and D. J. Adams, *Angewandte Chemie*, 2017, **129**, 10603-10606.
9. C. Colquhoun, E. R. Draper, R. Schweins, M. Marcello, D. Vadukul, L. C. Serpell and D. J. Adams, *Soft Matter*, 2017, **13**, 1914-1919.
10. E. R. Draper, M. Wallace, R. Schweins, R. J. Poole and D. J. Adams, *Langmuir*, 2017, **33**, 2387-2395.
11. E. R. Draper, B. Dietrich, K. McAulay, C. Brasnett, H. Abdizadeh, I. Patmanidis, S. J. Marrink, H. Su, H. Cui, R. Schweins, A. Seddon and D. J. Adams, *Matter*, 2020, **2**, 764-778.
12. S. Sathaye, A. Mbi, C. Sonmez, Y. Chen, D. L. Blair, J. P. Schneider and D. J. Pochan, *Wiley Interdisciplinary Reviews-Nanomedicine and Nanobiotechnology*, 2015, **7**, 34-68.